Bachelor in Biomedical Engineering

Continuum Mechanics and Structural Analysis Department

Universidad Carlos III de Madrid

Bachelor Thesis

Nonlinear Vibrations of an Idealized Saccular Aneurysm

Author:
Clara Ramón Lozano

Tutors:
Damián Aranda Iglesias
José Antonio Rodríguez Martínez

Leganés, July 2017

This page was intentionally left blank

Agradecimientos

En primer lugar me gustaría mostrar mi agradecimiento a mis tutores, Jose y Damián. Gracias Jose por ofrecerme la posibilidad de realizar este trabajo y enseñarme un campo que nunca habría pensado que me llamaría tanto la atención. Gracias Damián por dedicar tantas horas a enseñarme una pequeña parte de todo lo que sabes. A los dos, muchísimas gracis, he aprendido un montón gracias a vosotros.

Este trabajo simboliza el fin de estos cuatro años de grado y por ello me gustaría acordarme de todos los que han formado parte de ellos. Gracias a todas las "Bioguapas" por estos cuatro años juntas y por todos esos momentos dentro y fuera de clase. En especial gracias a Elena, por ser mi compañera de "fregaos" desde el primer momento. Gracias también a lo de dele, a los bio y a los no bio, porque siempre habrá alguien disponible para cualquier plan que se nos ocurra, por raro que pueda ser. Y por último, gracias a todos los de CEEIBIS, por todas nuestras tardes de trabajo y de no trabajo que hemos pasado en la universidad.

Gracias a Baldo, por darme siempre otro punto de vista y por querer compartir conmigo tantos proyectos. Gracias por ayudarme y comprenderme siempre que lo necesito.

Por último, gracias mis padres y mi hermana, por apoyarme siempre en cualquier decisión que tomara y por incitarme a buscar siempre aquello que me guste. Gracias a ti mamá, por preguntarme todos los días cómo me ha ido el día y por ofrecerte en cualquier momento a que te cuente que es lo que estoy haciendo. Gracias a ti papá, por todas esas conversaciones "freakes" que durante todos estos años hemos compartido y por transmitirme esa pasión por entender el por qué de todo.

Gracias.

This page was intentionally left blank

Abstract

Intracranial saccular aneurysms are a small portion of a vessel that bulges outward forming a balloonlike sac. Approximately 3% of the worldwide population suffer from this pathology and its rupture entails subarachnoid haemorrhage, causing in most of the cases brain damage or even death. Many physical and clinical factors such as its location, geometry and growth, the surrounding fluids, other underlying condition, the sex or the age of the subject highly affect the evolution of aneurysms. However, although it is known that many parameters affect their development, the main criteria for deciding their treatment is their size.

The main contribution of this work is the development of a 3D mathematical model to describe the behaviour of an idealized intracranial saccular aneurysm. An study of its mechanical behaviour is performed to understand under which conditions the aneurysm will break. The problem is divided into three main sections: the first one considers an aneurysm surrounded by a non-viscous Newtonian fluid and a constant internal pressure, the second one introduces the viscosity in the surrounding fluid and the last one introduces an internal pulsatile pressure. Additionally, this work analyzes how the variations of the internal pressure value, the thickness of the aneurysm and the density of both the surrounding fluid and aneurysm's wall, affect the behaviour of the aneurysm.

This page was intentionally left blank

Keywords

Intracranial saccular aneurysm, Cerebrospinal fluid, Pulsatile blood pressure, Finite elasticity, Non-linear vibrations

This page was intentionally left blank

Contents

Agradecimientos **iii**

Abstract **v**

Keywords **vii**

Contents **ix**

List of Figures **xi**

1 Introduction **1**
1.1 Context 2
1.2 Motivation and Objectives 3
1.3 Socio-Economic Impact 3

2 Theoretical Background **5**
2.1 Aneurysms: Theoretical Background 5
2.2 State of the Art 10

3 Problem Formulation **13**
3.1 The Aneurysm's Wall 14
3.2 Pressure Derivation 16
3.2.1 Blood pressure 16
3.2.2 Cerebrospinal fluid 17
3.2.3 Total pressure 18
3.3 Non-linear Governing Equation 18
3.4 Balance of Mechanical Energy 20
3.5 Analitical Solution 21
3.6 Numerical Solution 22

4 Constitutive Modelling **23**

5 Results **25**
5.1 Aneurysm's Model: Non-Viscous CSF and Constant Internal Pressure . 25
5.2 Aneurysm's Model: Viscous CSF and Constant Internal Pressure . . . 32
5.3 Aneurysm's Model: Viscous CSF and Pulsatile Internal Pressure 33

6 Conclusions and Future Work **37**
6.1 Conclusions 37
6.2 Future Work 39

A Derivation of Equations **41**
A.1 Proof: Balance of Linear Momentum for a Spherical Volume Element . 41
A.2 Proof: Kinematics Relationships 43
A.3 Proof: Pressure Exerted by the Cerebrospinal Fluid 47
A.4 Proof: Energy Terms 50

B Regulatory Framework and Budget **55**
B.1 Regulatory Framework 55
B.2 Budget 56

References **59**

List of Figures

2.1 Types of cerebral aneurysms. *Source: Joseph [30]* 6

3.1 Schematic representation of an idealized saccular (spherical) aneurysm surrounded by cerebral spinal fluid and subjected to radially symmetric pulsating blood pressure. 13

5.1 Aneurysm's model for constant internal pressure and zero viscosity for various dimensionless pressures. 27

5.2 Aneurysm's model for constant internal pressure and zero viscosity for various dimensionless radius. 28

5.3 Aneurysm's model for constant internal pressure and zero viscosity varying dimensionless density. Analysis of energies for Neo-Hookean model. 30

5.4 Aneurysm's model for constant internal pressure and varying dimensionless viscosity. 32

5.5 Variation of dimensionless pressure with time, stretch variation with time and phase diagram for variable internal pressure. 34

A.1 Infinitesimal spherical element. 41

B.1 Detailed budget for the current project. 57

Chapter 1

Introduction

According to Tortora and Derrickson [52], an aneurysm is "a thin, weakened section of the wall of an artery or a vein that bulges outward, forming a balloonlike sac." They can appear in different regions of the body, and according to their location they can be classified as aortic, cerebral or peripheral aneurysms [39] Nowadays in the United States, approximately 6 million people suffer from intracranial aneurysms, meaning that 1 out of 50 people in the USA suffer from this condition [8].

Understanding how aneurysms work has been a major priority for their early diagnosis. The refinement of the detection of aneurysms will allow physicians to prevent the rupture of aneurysms and to minimise the risks when an intervention is needed for their removal. In the field of biomechanics, approaches to understand how they grow, how they evolve over time or how the surrounding parameters affect their behaviour have been performed.

Along this work, a structural analysis of how an idealised intracranial saccular aneurysm behaves under different constitutive models, varying different characteristics and surrounding conditions is developed in order to try to clarify how and when a rupture of the aneurysm will occur. Chapter 1 starts contextualizing aneurysms, which is their impact in society, followed by the objectives of this work and how its results will affect society. Then, in chapter 2, a brief background about aneurysms, the different existing types and which factors affect their rupture is given. The state of the art, which constitutes a summary of the different works in modelling intracranial aneurysms, is also presented there. In chapter 3 the formulation of the problem addressed in this research work is performed and in chapter 4 the different constitutive models are described. Finally, chapters 5 and 6 present the obtained results and the conclusions and future work respectively. The budget and regulatory framework are included in the annexes, next to the detailed explanation of specific sections from the problem formulation.

1.1 Context

Nowadays, unruptured intracranial aneurysms have a prevalence of 3% in worldwide population [15]. Most common symptoms involve localized headache, dilated pupils, blurred or double vision, pain above or behind the eyes, weakness and numbness or difficulties in speaking [8]. However, about 95% of the cerebral aneurysms are asymptomatic [38], hardening early detection. When subarachnoid haemorrhages (SAH) results from the breakage of aneurysms, besides the previous symptoms, patients might experiment a really severe headache, loss of consciousness, nausea and vomiting, stiff neck, change in mental status, dizziness, photophobia, a seizure or even sudden death. About 1%-3% of non-symptomatic aneurysms bleed annually and in about 70% of the patients vasospasm (narrowing of the vessels due to vasoconstriction) occurs.

In 1992, Wiebers et al. [57] analysed the impact of aneurysms in the population of United States. They estimated that about 10,300 patients were hospitalised every year with unruptured intracranial aneurysms. The estimated cost was of $522,500,000, which is a negligible cost when compared to the cost of patients with subarachnoid haemorrhages (SAH), which implied a cost of $1,755,600,000 annually. Another study from 1997 [38] reflected from autopsy data that about 5 million individuals in North America had intracranial aneurysms, among them 28,000 ruptured every year. The saccular aneurysms were found in 2% of the autopsy population and between the 20% and 30% of the cases appeared with multiple saccular aneurysms.

However, a slight decrease in subarachnoid haemorrhages derived from the rupture of aneurysms has been found between 1950 and 2005, probably because of the reduction in smoking habits[1] and the early detection and treatment [55]. In 2010 in Spain, 1.10% of the total population suffered from deep brain damage caused from the rupture of a cerebral aneurysm [43]. If this percentage is further analysed, 1.17% of the affected individuals are women whereas men constitute a 1.04%.

A more recent study performed by Asaithambi et al. [3] shows that 15.6 out of 100,000 persons suffer from unruptured intracranial aneurysms, being 7.7 out of 100,000 experimenting SAH. However the largest prevalence occurs in people aged 75-84, which constitute 61.6 persons out of 100,000. The SAH rate is also higher, being 30.1 persons out of 100,000 older than 85 years old. Other studies reported a higher incidence in women, being 22.5 out of 100,000 affected by unruptured intracranial aneurysms and 9.6 by SAH. However, they estimated that by 2018 in USA a budget of $4.4 trillion would be needed, which will represent a 20% of the Gross Domestic Product [2].

[1] Smoking, with hypertension, has a great impact in the growth and rupture of intracranial aneurysms, as it will be explained later in chapter 2

[2] GDP is the monetary value of all the goods and products produced by a country in a specific time period [26].

1.2 Motivation and Objectives

Due to the prevalence of intracranial aneurysms, there is a need for studying and understanding how aneurysms evolve. A correct detection and treatment will improve the survival rate of individuals suffering from this condition. As it will be presented later, the rupture of an aneurysm will occur depending on the aneurysm's wall structure and its surrounding factors.

So, due to its prevalence and geometry, this project has selected an intracranial saccular aneurysm for performing the dynamic analysis that will bring to light some of the features affecting the growth and rupture of this type of aneurysms. Consequently, the aim of this project is:

- To develop a mathematical model to study the non-linear vibrations of an idealized saccular aneurysm surrounded by the cerebrospinal fluid (CSF).
- Analyse how different biological and directly-related parameters affect the behaviour of an aneurysm.
- Compare how the system behaves under two different constitutive models and see the strong dependencies between the material parameters.

In the parametric analysis the characteristics that are going to be tested are the density of the aneurysm's wall and of the cerebrospinal fluid, the pressure exerted by the circulating blood flow and the difference in thickness of the aneurysm. It is analyzed too how is the dynamic behaviour of the aneurysm given there is a viscous contribution coming from the surrounding fluid. It is also included a pulsatile internal pressure to see how it affects the behaviour of the aneurysm's wall. Moreover, during the parametric analysis the two constitutive models that are going to be employed are the Neo-Hookean model and a Mooney-Rivlin model of three parameters, both calibrated for aneurysmal tissue according to the data of Costalat et al.[13].

1.3 Socio-Economic Impact

A deeper understanding of the dynamics of intracranial saccular aneurysms could optimize the future treatment of patients suffering from this alteration. Although this research is just a first step in the understanding of the development of this type of aneurysms, it is accurate enough to clarify how the different biological parameters are affecting their growth. Future works will consider all the parameters affecting the development of intracranial saccular aneurysms and they will include more accurate constitutive models describing the tissue. All this information will allow physicians to

compare the data obtained by imaging techniques with the complementary information reported by the model.

Nowadays, one of the main problems in this area is the lack of experiments. A larger amount of experiments over aneurysm's walls will allow an improvement of constitutive models. Although this work develops a mathematical model for the dynamic behaviour of spherical shells, it is highly influenced by the constitutive model, as will be introduced later in chapter 5. The constitutive model describes the mechanical behaviour of the aneurysm's wall but one of the main problems of biological tissue is that it remodels by itself much faster than other known inert material. Consequently, really accurate experiments must be performed in order to register all the different conformations an aneurysm's wall achieve during its life cycle. The lack of those models and the reduction of the geometry of the proposed problem make this work hardly useful for early diagnosis and prediction of when the aneurysm will break.

However, for developing more sophisticated models that will allow the prediction of the rupture of aneurysms some bases have to be set. This work is a first approach in the understanding of how different biological parameters affect the development of aneurysms and can be considered as a first step for future models. Improvement of *in-vivo* diagnosis techniques will allow to study the conformation of the aneurysm's wall, returning some information that could be applied to the mathematical model. This will provide physicians with another tool for contrasting information and predict whether the aneurysm will break or not.

The use of a mathematical model for deciding whether an aneurysm is surgically removable or not will improve the survival rate of affected individuals. Nowadays the main criteria for deciding whether an aneurysms is operable or not is mainly its size, discarding the removal of many aneurysms under 5 mm of diameter. However, in many cases these aneurysms break and cause a really severe haemorrhage that leaks into the subarachnoid space (see section 2.1). Thus, the inclusion of mathematical models into the diagnostic procedure as a complementary technique to the already standard ones will reinclude for consideration aneurysms that in other cases will not receive a correct treatment. By this way, these aneurysms will be traced with more attention by physicians or even surgically removed in case some new hazardous indices appear.

Moreover, using reliable mathematical models describing the growth of such biological structures will not only improve the survival rates for people having aneurysm, but they also will save considerable amounts of money to the government. As presented before, the overall cost of patients having a ruptured aneurysms triplicates the cost of those with an unruptured one. Furthermore, patients suffering sequels from the SAH will require more resources from the government or insurance companies. In summary, a proper diagnosis and removal of intracranial saccular aneurysms will diminish extra costs derived from patients suffering the effects of an avoidable SAH.

Chapter 2

Theoretical Background

2.1 Aneurysms: Theoretical Background

As presented before, aneurysms are outpouchings in the wall of an artery or a vein. Depending on their location, they can be classified in different subgroups [39]:

- **Aortic aneurysms:** divided into abdominal aortic and thoracic aortic, depending in which region of the aorta they are found.
- **Cerebral aneurysms:** located in the brain, they normally produce no symptoms until they become large.
- **Peripheral aneurysms:** all those aneurysms located in arteries different from the aorta or the brain ones. Normally their rate of rupture is lower than the aortic ones but a clot detached may be fatal for the patient.

This study has been developed for intracranial saccular aneurysms so this brief introduction is focused in understanding the different types of brain aneurysms, how they grow and break and what are the factors affecting their rupture.

A cerebral aneurysm is a small dilatation of an artery or vein from the brain and between 3% and 5% of the global population suffer from them [12]. There are different types of cerebral aneurysms depending on their shape and cause of formation. Mycotic aneurysms are usually formed after a bacterial infection whereas fusiform aneurysms usually result from atherosclerosis and are located at the vertebrobasilar and internal carotid artery regions [38]. Also some aneurysms appear because of some trauma or because of the appearance of some tumor [46]. The other two types found are dissecting aneurysms, found in the extracranial arteries, and saccular aneurysms [38], which are the most common cerebral aneurysms and also seem to be the most common cause

of non-traumatic subarachnoid haemorrhage [12, 36]. Notice that the breakage of the aneurysm produces a leak of blood into the subarachnoid space, leading to some severe health issues that may also lead to death.

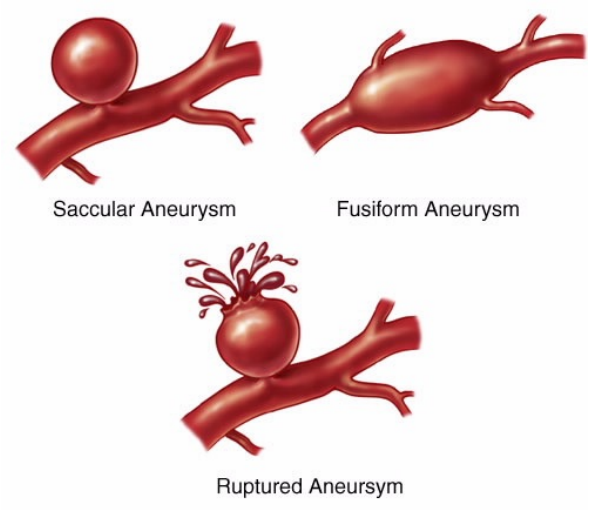

Figure 2.1: Types of cerebral aneurysms. *Source: Joseph [30]*

The growth of intracranial saccular aneurysms is highly related to the histologic structure of the arteries where the appears. Cerebral arteries, as other along the body, are formed by three main layers: tunica intima, tunica media and adventitia. Adventitia is the most outer layer of the artery wall and is mainly composed of connective tissue which also anchors the vessel to the tissues of the surroundings. The layer of the middle, the tunica media, is mainly formed of smooth muscle in the case arteries located in the brain but also some layers of elastic tissue appear in some other arteries. Finally the inner layer, the tunica intima, is composed of a thin layer of endothelium, the basement membrane and variable amounts of connective tissue. So, depending on the composition and condition of those layers, aneurysms will be prompt to appear or not and to break or not.

Saccular aneurysms commonly appear in the bifurcations of the arteries, where the muscular layer weakens or even disappears [12, 17, 45, 46]. Then, tunica intima and tunica media must be absent or really weakened in order for the aneurysms to form and break. More recent studies [12, 18] have shown that one of the main processes involved in the disappearance of those layers is inflammation, where the apoptosis of smooth muscle is induced and consequently, the extracellular matrix that is protecting the vessel's wall is destroyed since smooth muscles cells are one of the most important synthesizers of this layer. Moreover, the formation of thrombus in the interior surface of the aneurysm wall enhances its degradation and consecutive rupture [18]. However, although the inflammatory process is highly related with the weakening of the vessel's wall, the question is which factors are provoking this inflammation and how can be known how and when the aneurysms will break, which seems not to follow a standard procedure or set of conditions.

Many studies have been developed to understand which factors affect the development of aneurysms, going from more physical parameters to those more related with genetics or even environmental factors.

Location

It has been studied whether the location of the aneurysms in the brain is correlated with the rupture of aneurysms. Although this phenomena occurs in different areas of the brain, Sandasivan et al. [45] showed that between 70% and 75% of ruptures occur in three areas: the middle cerebral artery, the posterior communicating artery and the anterior communicating artery, which seem to show some correlation between the possible rupture and its location.

Geometry and Growth

Growth increases considerably the risk of rupture. Risk of rupture was found to be 2.4% in aneurysms with growth versus only 0.2% in those without growth [54]. Some factors driving aneurysm's growth are inflammation and matrix degeneration but it is also highly influenced by the initial size of the aneurysm and some habits as tobacco smoking [12].

From different studies it seems that the size of the aneurysm also matters, being those between 5 and 10 mm the ones with higher risk of rupture [45]. In general, an increase in the size entails an increase in the risk of rupture [18]. However, some aneurysms with an overall size smaller than 5 mm are associated with large and severe subarachnoid haemorrhage [9, 42]. Nevertheless, this information is not so accurate for predicting the rupture of aneurysm since the mean difference in size between ruptured and unruptured ones is of at most about 1.5 mm [45]. Other parameters that can be used to describe the rupture of an aneurysm are neck, depth, surface area, volume or aspect ratio [53].

So, the aspect ratio (ratio of size in different dimensions), considered to be a more precise parameter when predicting the rupture of aneurysms, is around 1.6 for unruptured aneurysms and 2.4 for ruptured ones [12, 45]. Ruptured aneurysms tend to have an irregular surface as well as those with a high bottleneck factor and height to width ratio (long and thin). Finally, a quite useful factor to consider the development of small aneurysms will be the aneurysms to vessel size ratio.

Shape is also influencing whether aneurysms will break or not. Multilobular aneurysms and those with non-spherical geometry are more prompt to break. In addition, those to which blood flow is penetrating directly will fail more easily [9].

Prediction based in size and growth is around 70% - 75% [45] but more data and parameters must be considered for an accurate prediction.

Flow

Blood flow has a great impact in the creation of aneurysm. Hemodynamics is the initiating factor for the formation of a cerebral aneurysm, easily seen in regions undergoing high hemodynamics stresses as bifurcations or abrupt angles of the vessels [12]. It is also known that non-physiological flow conditions can cause wall deterioration, ending with the loose of endothelium. In addition, the variations in geometry of the aneurysm may vary the wall shear stress conditions created by the fluid, ending in more deterioration and de-endothelialization of the wall[18].

As presented before, saccular aneurysms commonly appear in areas where the wall is subjected to a higher stress by the incoming flow, such as bifurcations of the arteries [11]. Although the pressure and flow exerted over the internal wall of each aneurysm vary with its geometry and for each patient, it can be considered that the pulsatile blood pressure is the same in the systemics regions and in the cerebral one but with some attenuation [45].

Genetics and Clinical Factors

In the most recent years it has been studied whether if there exists a correlation between the breakage of an aneurysm and having some genetic related disease. It has been found that some individuals having genetic diseases are more prompt to develop an aneurysm. Some of the diseases related are Ehlers-Danlos type IV, a rare syndrome where individuals have muscular weakness, or autosomal dominant polycystic kidney disease, one of the most common hereditary diseases. Individuals having those diseases conform between 10% to 13% of the population having cerebral aneurysms [9, 12]. Some other as fibromuscular dysplasia and Marfan syndrome affects the development of intracranial aneurysms, as well hypertension, the family history and the ageing, that also have an important impact in the appearance of aneurysm. In conclusion, people with comorbidity tends to have a higher probability of developing aneurysms [55].

Some studies considering ruptured and unruptured aneurysms have correlated some genes involved in the degradation of the vessel's wall as well in the inflammation process [18]. Hence, it has been seen in practice that genetic therapy resulted in the prevention of aneurysm rupture, as for example by activating the macrophages in the area [12].

Another factor mentioned before, has been a case of study in many researches directed to understand the rupture of intracranial aneurysms. Hypertension is thought to be a major cause of the aneurysms growth as well as of a non-correct repair of its wall [9]. Hypertension also increases blood pressure, what in some patients increases the

wall shear stress by 4.2%, resulting in an increase of a 14.5% - 17.5% of the area of the intracranial aneurysm [50]. Overall, people who have been treated for hypertension at some point in their lives shows more than three times more possibilities of developing a SAH [4, 7].

Smoking also influences the appearance and growth of cerebral aneurysms. Actually, cigarette smokers have five times more risk of ending with the rupture of aneurysms than non-smokers. This habit weakens the arterial wall, predisposing them to develop an aneurysm [2, 7, 9, 50]. Furthermore, if some individuals are having some specific gene variations related to the formation of aneurysms, the risk of developing such deformation in the wall increases dramatically. In contrast, regular physical exercises decrease the risk of developing one [12].

No clear evidence has been found that allow the community to correlate the appearance and rupture of aneurysms with the country where patients belong [55].

Age and Sex

Finally, different studies have been developed to prove that age and gender affects the aneurysm's formation. In general, a higher risk of developing cerebral aneurysms is attributed to females. Specifically, women between the perimenopausal and post-menopausal periods are found to be more prompt to develop an aneurysm. However, since estrogens protect against the formation and growth of aneurysms but they experiment a decrease during menopause in women [9], hormonal therapies have been proved to protect from the SAH resulting from the rupture of aneurysms [12, 55]. Furthermore, due to anatomical and physiological variations, the wall shear stress in the bifurcations located in the middle cerebral artery is 17% higher in women than in men whereas in the internal carotid artery is 50% higher, resulting in a higher pressure over the vessel's wall [33]. Moreover, women with smoking habits undergo more possibilities of having an aneurysmal SAH [2].

With respect to the influence of age in the development and rupture of aneurysms, some studies postulated that the risk of rupture rises with age, reaching a plateau in older ages or even decreasing after the age of 50 [9]. Others as Vlak et al. suggested that there is an inflexion point at the age of 30, where the prevalence of aneurysms increases considerably [55]. However, some authors as Lindekleic et al. [33], concluded that there is no strong correlation between the age and the risk of rupture of aneurysms.

2.2 State of the Art

From the previous analysis of the parameters affecting the rupture of aneurysms, it has been seen that it is highly affected by the geometry and size. Thereby, it is one of the major criteria for deciding the future treatment of an aneurysmal patient. The fail of the wall of the aneurysm is also affected by all the parameters presented before but is just the combination of all what will determine whether an aneurysm will break or not. Consequently, a study in the mechanical behaviour of the aneurysm's wall will bring to light how and under which conditions the aneurysm might break.

Notice that in this work the word bifurcation appears with two different meanings. In the first part bifurcations refereed to the division of one vessel into two different branches whereas from now on, it will refer to the end of oscillatory motion in the mathematical model describing the behaviour of the aneurysm. On this last case, bifurcation can be matched physically with the rupture of the aneurysm's wall.

The question of whether mechanical instabilities, both static and dynamic, may cause the enlargement and rupture of saccular aneurysms has been debated by the scientific community during the last 40 years. Several researchers, such as Akkas [1] and Austin et al. [5], signalled that the existence of limit point instabilities (i.e. mathematical bifurcations occurring in the quasi-static response of the aneurysm) could be a reason for the growth and rupture of this type of lesions.

Alternatively, other authors like Jain [28], Sekhar and Heros [46] and Sekhar et al. [47] suggested that the pulsatile blood flow could excite the natural frequency of the aneurysm making it dynamically unstable. This hypothesis was supported by the results of Simkins and Stehbens [49] and Hung and Botwin [25], who studied the elastodynamics of berry (saccular) aneurysms and showed that the natural frequency of these type of lesions may lie within the range of bruit frequencies that commonly accompany aneurysms. However, despite the nonlinear stress-strain response exhibited by the aneurysm's wall over finite strains, these authors used in their analysis the classical shell membrane theory [1], which assumes infinitesimal strains and linear material behaviour. Furthermore, they ignored the contribution of the Cerebral Spinal Fluid (CSF) surrounding the lesion. Thus, the idea that resonances may cause the rupture of intracranial aneurysms has been gradually losing support within the scientific community.

Shah and Humphrey [48] and David and Humphrey [14] studied the nonlinear elastodynamics of a sub-class of spherical aneurysms subjected to pulsatile blood pressure and surrounded by CSF. The aneurysmal wall was modelled using a Fung-type

[1]The shell membrane theory stands that for sufficiently small thickness the stresses acting over this direction can be negligible [20]

pseudostrain-energy function which included strain rate dependence. These works brought to light that both surrounding fluid and material viscosity help to increase the dynamic stability of the aneurysm. Shortly after, Haslach and Humphrey [22] provided further insights into the effect of the mechanical behaviour of the aneurysmal wall on the dynamic response of the lesion. Through the comparison of various strain energy functions, the authors pointed out the great sensitivity of the dynamic behaviour of the aneurysm to the constitutive model used to describe the aneurysmal wall. In particular, they stressed the fact that it is essential for the (correct) analysis of the dynamic stability of aneurysms to use constitutive models specifically formulated and calibrated for the aneurysmal wall. It was shown that the opposite may give rise to misleading results which predict dynamic instabilities that there are not present in actual tissue.

Nevertheless, the work by Humphrey and co-workers [14, 22, 48] had been developed in a 2-D framework. While many aneurysmal lesions show small wall thickness and thus can be modelled relying on the membrane hypothesis, the necesity of using a 3D formulation arises from the works of Suzuki and Ohara [51], MacDonald et al. [34] and Costalat et al. [13] who obtained experimental evidences of intracranial aneurysms with a ratio between wall thickness and inner radius larger that 0.1, leading to non-negligible radial stresses through the aneurysmal wall.

So, due to the necessity of developing a three dimensional framework to describe the dynamic behaviour of an intracranial saccular aneurysm based on the strong evidence given by some authors [13, 34, 51], this project extends the work done by Humphrey and co-workers [14, 22, 48] and develops it for an idealised saccular aneurysms surrounded by an external fluid, discarding then the shell membrane theory. For two different constitutive models, a parametric analysis of different affecting variables as the density of the wall and the surrounding fluid, viscosity of the CSF, the radius of the aneurysm and the variable internal pulsatile pressure is performed in order to clarify how this parameters affect the bifurcation of the aneurysm and how is the dependency between different constitutive models.

Chapter 3

Problem Formulation

In this chapter, the mathematical framework employed to model the problem of an idealized saccular (spherical) aneurysms is presented. The aneurysm's model will be then tested for different situations according to the cerebrospinal fluid conditions. In the most basic aneurysm's model analyzed, the walls are surrounded by a non-viscous incompressible Newtonian fluid and subjected to an internal constant blood pressure. Thereafter, the viscosity of the fluid is included and finally, a pulsating radially symmetric blood pressure affecting the internal wall of the aneurysm (see figure 3.1) is also incorporated.

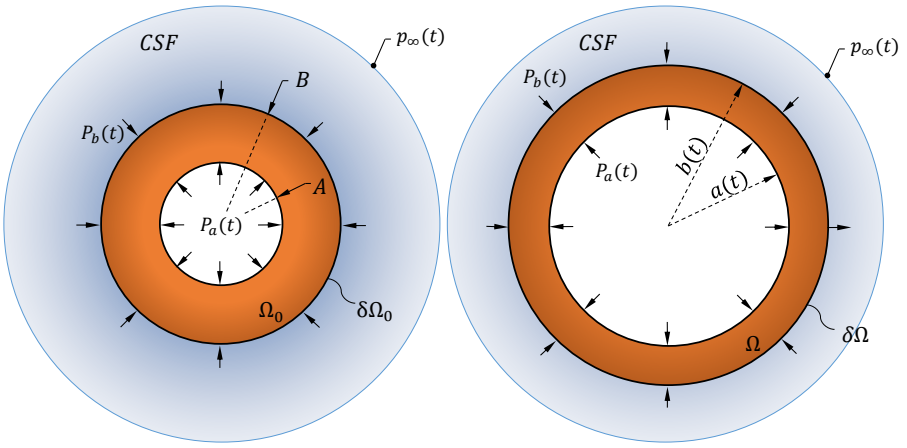

Figure 3.1: Schematic representation of an idealized saccular (spherical) aneurysm surrounded by cerebral spinal fluid and subjected to radially symmetric pulsating blood pressure. (a) Reference and (b) deformed configurations.

The contribution of this work is to extend the 2D formulation developed by Humphrey and co-workers [48, 14] to a 3D framework. As presented before, the motivation for a 3D formulation comes from the data provided by Costalat et al. [13], who pointed out that the ratio between thickness and radius of intracranial aneurysms may be larger that 0.1, leading to non-negligible radial stresses through the aneurysm's wall (see chapter 5).

3.1 The Aneurysm's Wall

Following the work of Shah and Humphrey [48], the aneurysm's wall is taken to be incompressible and isotropic within the framework of finite non-linear elasticity. While the hypothesis of homogeneous and isotropic properties is likely a gross approximation [44], it is correct enough to study the elastodynamics of the aneurysmal lesion [23].

So, the aneurysms occupies a volume Ω_0 defined by the spherical polar coordinates (R, Θ, Φ) in some reference configuration such that $A \leq R \leq B$, being A the inner radius of the sphere and B the outer radius. In this work $A = 4.3$ mm and $B = 4.67$ mm are taken which, based on the work of Costalat et al. (2011), represent average values for the inner and outer radii of intracranial aneurysmal lesions. Since the material is deformed so that the spherical symmetry is maintained, the motion is given by

$$r = r(R, t); \qquad \theta = \Theta; \qquad \phi = \Phi \tag{3.1}$$

where (r, θ, ϕ) are spherical polar coordinates in Ω configuration such that $a \leq r \leq b$, being a the inner deformed radius and b, the outer deformed one, see figure 3.1.

From the second Newton's law $\sum \vec{F} = m\vec{a} = \rho \, \mathrm{d}V \ddot{\vec{r}}$ and setting the equilibrium for an spherical volume element whose $\mathrm{d}V = r^2 \cos\phi \mathrm{d}r\mathrm{d}\theta\mathrm{d}\phi$, the balance of linear momentum in the radial direction results as equation (3.2) [1]

$$\frac{\partial \sigma_r}{\partial r} + 2\frac{(\sigma_r - \sigma_\theta)}{r} = \rho \ddot{r} \tag{3.2}$$

where a superposed dot denotes differentiation with respect to time, $\sigma_r(r, t)$ and $\sigma_\theta(r, t)$ are the radial and circumferential Cauchy stresses respectively and $\rho = 1050$ kg/m^3 is the density of the aneurysm's wall [48].

[1] For the complete derivation of equation (3.2), see appendix A.1.

Now, let $\lambda_r = \frac{\partial r}{\partial R}$ and $\lambda_\theta = \lambda_\phi = \frac{r}{R} = \lambda$ denote the radial and circumferential stretches respectively. From the incompressibility condition ($\lambda_r \lambda_\theta \lambda_\phi = 1$) it is deduced that

$$\lambda(r,t) = \left(\frac{B^3}{R^3}(\lambda_b^3 - 1) + 1\right)^{1/3} \tag{3.3}$$

where $\lambda_b = \frac{b}{B}$ stands for the circumferential stretch in the outer surface of the aneurysm's wall. The derivatives of equation (3.3) with respect to r and t are taken to obtain respectively

$$\frac{\partial \lambda}{\partial r} = -\frac{\lambda^3 - 1}{R} \tag{3.4}$$

$$\ddot{\lambda} = \frac{\lambda^3 - 1}{\lambda_b^3 - 1}\left(\frac{2\lambda_b \dot{\lambda_b}^2 + \lambda_b^2 \ddot{\lambda_b}}{\lambda^2} - \frac{2\,\lambda_b^4 \dot{\lambda_b}^2}{\lambda^5}\frac{\lambda^3 - 1}{\lambda_b^3 - 1}\right) \tag{3.5}$$

Notice that when λ appears with some superimposed dots it means a derivative of the stretch λ over time. By introducing the equations above (equation (3.4) and (3.5)) into equation (3.2), the balance of linear momentum results as:

$$\frac{\partial \sigma_r}{\partial \lambda} - 2\frac{\sigma_r - \sigma_\theta}{\lambda(\lambda^3 - 1)} = \rho B^2 \left(\frac{2\,\lambda_b^4 \dot{\lambda_b}^2}{(\lambda_b^3 - 1)^{4/3}}\frac{(\lambda^3 - 1)^{1/3}}{\lambda^5} - \frac{2\lambda_b \dot{\lambda_b}^2 + \lambda_b^2 \ddot{\lambda_b}}{(\lambda_b^3 - 1)^{1/3}}\frac{1}{\lambda^2(\lambda^3 - 1)^{2/3}}\right) \tag{3.6}$$

From the work of Ogden [40], it is known that for an incompressible spherical shell

$$\sigma_r - \sigma_\theta = -\frac{1}{2}\lambda \frac{d\psi}{d\lambda}(\lambda^{-2}, \lambda, \lambda) \tag{3.7}$$

where ψ is the strain energy function which determines the mechanical behaviour of the material, which will be defined later in chapter 4. In addition, from the work by Shah and Humphrey [48] it is known that:

$$\sigma_r\,(r,t) = \begin{cases} \mathrm{P_a}, & \mathrm{r = a} \\ \mathrm{P_b}, & \mathrm{r = b} \end{cases}$$

so, with the help of equation (3.7), if equation (3.6) is integrated over the thickness of the aneurysm, equation (3.8) results:

$$P_b - P_a + \int_{\left(\frac{\lambda_b^3+f_0-1}{f_0}\right)^{1/3}}^{\lambda_b} \frac{\psi'(\lambda)}{\lambda^3-1}\mathrm{d}\lambda = \rho B^2 \left(\lambda_b \ddot{\lambda_b} \left(\frac{\lambda_b}{(\lambda_b^3+f_0-1)^{1/3}} - 1\right)\right) - \\ - \rho B^2 \left(\dot{\lambda_b}^2 \left(\frac{\lambda_b^4}{2(\lambda_b^3+f_0-1)^{4/3}} - \frac{2\lambda_b}{(\lambda_b^3+f_0-1)^{1/3}} + \frac{3}{2}\right)\right) \tag{3.8}$$

where the superscript prime denotes differentiation with respect to the circumferential stretch. Moreover, $f_0 = \frac{A^3}{B^3} = 0.78$ is a dimensionless parameter which characterizes the thickness of the aneurysm's wall and $P_a(t)$ and $P_b(t)$ are the blood pressure and the pressure exerted by the CSF on the aneurysm respectively, whose specifics forms will be derived later in section 3.2. So equation (3.8) will be the final expression for the balance of linear momentum [2].

3.2 Pressure Derivation

3.2.1 Blood pressure

As presented at the beginning of chapter 3, two different situations for the internal pressure are employed. First, a constant pressure such as

$$P_a = P_m \tag{3.9}$$

where $P_m = 65.7\,\mathrm{mmHg}$ [48] (varied during the parametric analysis).

Then, based on the data measured by Ferguson [16] for human saccular aneurysms and assuming that the pressure is uniform inside the lesion, the pulsating radially symmetric blood pressure is represented by the following Fourier series

$$P_a(t) = P_m + \sum_{n=1}^{N} \left(A_n \cos(n\omega t) + B_n \sin(n\omega t)\right) \tag{3.10}$$

where $P_m = 65.7\,\mathrm{mmHg}$ is the mean pressure, A_n and B_n are the fourier coefficients for N harmonics, and ω is the fundamental circular frequency. Following the work of Shah and Humphrey [48], the 5 harmonics are: $A_1 = -7.13$, $B_1 = 4.64$, $A_2 = -3.08$, $B_2 = -1.18$, $A_3 = -0.130$, $B_3 = -0.564$, $A_4 = -0.205$, $B_4 = -0.346$, $A_5 = 0.0662$ and $B_5 = -0.120$, have been considered. All quantities are given in mmHg.

[2] For the complete derivation of equation (3.8), see appendix A.2

3.2.2 Cerebrospinal fluid

Considering the Cerebrospinal Fluid (CSF) to be an incompressible and Newtonian fluid, the continuity equation takes the form

$$\frac{1}{r^2}\frac{\partial}{\partial r}(r^2\, v_r) = 0 \tag{3.11}$$

implying that the radial velocity is $v_r(r,t) = \frac{c(t)}{r^2}$. The function $c(t)$ is found matching the fluid and aneurysm's wall velocities at the outer surface of the aneurysm's wall such that $r = b$. Thus, it is obtained the following expression, which relates the radial velocity of the CSF and the stretch (and stretch rate) in the outer surface of the aneurysm

$$v_r(r,t) = \frac{B^3\lambda_b^2\dot{\lambda}_b}{r^2} \tag{3.12}$$

Moreover, the balance of linear momentum along the radial direction takes the form

$$\rho_f\left(\frac{\partial v_r}{\partial t} + v_r\frac{\partial v_r}{\partial r}\right) = -\frac{\partial p}{\partial r} + \mu\left(\frac{1}{r^2}\frac{\partial}{\partial r}\left(r^2\frac{\partial v_r}{\partial r}\right) - 2\frac{v_r}{r^2}\right) \tag{3.13}$$

where $\rho_f = 1000\,\mathrm{kg/m^3}$ and $\mu = 1.26\,10^{-4}\,\mathrm{Ns/m^2}$ are the density and viscosity of the CSF respectively [48] and p denotes pressure.

Next, by inserting equation (3.12) into equation (3.13), equation (3.14) is obtained

$$\frac{\partial p}{\partial r} = -\rho_f\left(\frac{B^3}{r^2}\left(2\lambda_b\dot{\lambda}_b^2 + \lambda_b^2\ddot{\lambda}_b\right) - 2B^6\frac{\lambda_b^4\dot{\lambda}_b^2}{r^5}\right) \tag{3.14}$$

If equation (3.14) is integrated over the range $r \in (b,\infty)$, the expression for the pressure exerted by the CSF on the outer surface of the aneurysm results as

$$P_{b_f}(t) = p_\infty + \rho_f B^2\left(\frac{3}{2}\dot{\lambda}_b^2 + \lambda_b\ddot{\lambda}_b\right) \tag{3.15}$$

where $p_\infty = 3\,\mathrm{mmHg}$ is the remote pressure and it is assumed constant [48].

From the constitutive equations of incompressible Newtonian fluids it is known that the dynamic pressure (radial stress) caused by the deformation of the CSF on the aneurysm's wall is given by

$$P_{b_s}(t) = -4\mu\frac{\dot{\lambda}_b}{\lambda_b} \tag{3.16}$$

where μ is the viscosity of the CSF.

3.2.3 Total pressure

From the geometry of the problem it is known that the total pressure exerted by the cerebral spinal fluid on the outer surface of the aneurysm is

$$P_b(t) = P_{b_{s(t)}} - P_{b_f}(t) \tag{3.17}$$

So, the final pressure will be composed by the contribution of the internal fluid (blood flow) and the external surrounding fluid (CSF) i.e, $P(t) = P_a(t) + P_b(t)$. Hence, the final expression[3] for the total pressure results as

$$P(t) = P_a(t) - p_\infty - \rho_f B^2\left(\frac{3}{2}\dot{\lambda}_b^2 + \lambda_b\ddot{\lambda}_b\right) - 4\mu\frac{\dot{\lambda}_b}{\lambda_b} \tag{3.18}$$

3.3 Non-linear Governing Equation

Finally, the combinations of equations (3.8) and (3.18) results in the governing equation of the problem i.e., the final equation describing the deformation of an idealized saccular aneurysm subjected to internal and external pressure

$$\begin{aligned} P_a(t) - p_\infty = {} & \rho_f B^2\left(\frac{3}{2}\dot{\lambda_b}^2 + \lambda_b\ddot{\lambda_b}\right) + 4\mu\frac{\dot{\lambda_b}}{\lambda_b} + \int_{\lambda_b}^{\left(\frac{\lambda_b^3+f_0-1}{f_0}\right)^{1/3}} \frac{\psi'(\lambda)}{\lambda^3-1}d\lambda - \\ & - \rho B^2\lambda_b\ddot{\lambda_b}\left(1 - \frac{\lambda_b}{(\lambda_b^3+f_0-1)^{1/3}}\right) - \\ & - \rho B^2\dot{\lambda_b}^2\left(\frac{\lambda_b^4}{2(\lambda_b^3+f_0-1)^{4/3}} - \frac{2\lambda_b}{(\lambda_b^3+f_0-1)^{1/3}} + \frac{3}{2}\right) \end{aligned} \tag{3.19}$$

Then, the following non-dimensional length, mass and time scales have been introduced in order to pose the problem in non-dimensional form

[3]For the complete derivation of equation (3.18), see appendix A.3

$$[L] = B; \qquad [M] = \rho B^3; \qquad [T] = \sqrt{\frac{\rho B^2}{C_{\mathrm{N10}}}} \tag{3.20}$$

where C_{N10} is a material constant further discussed in section 4. Previous non-dimensional groups are applied to equation (3.19) to obtain the following dimensionless governing equation which shows that λ_b is the only unknown of the problem

$$\begin{aligned}\overline{\Delta P} = \int_{\lambda_b}^{\left(\frac{\lambda_b^3+f_0-1}{f_0}\right)^{1/3}} \frac{\overline{\psi}'(\lambda)}{\lambda^3-1}\, d\lambda + 4\kappa\frac{\dot{\lambda}_b}{\lambda_b} + \overline{\rho}\left(\lambda_b\ddot{\lambda}_b + \frac{3}{2}\dot{\lambda}_b^2\right) \\ -\lambda_b\ddot{\lambda}_b\left(1 - \frac{\lambda_b}{(\lambda_b^3+f_0-1)^{1/3}}\right) - \dot{\lambda_b}^{\,2}\left(\frac{3}{2} + \frac{\lambda_b^4}{2(\lambda_b^3+f_0-1)^{4/3}} - \frac{2\lambda_b}{(\lambda_b^3+f_0-1)^{1/3}}\right)\end{aligned} \tag{3.21}$$

where now a superposed dot denotes differentiation with respect to the dimensionless time. Note that when $f_0 \longrightarrow 1$ Eq. (12) of Shah and Humphrey [48] is recovered. For the case $P_a(t)$ defines a pulsatile flow, the dimensionless expression is

$$\overline{P_a}(\tau) = \overline{P_m} + \sum_{n=1}^{N}\left(\overline{A_n}\cos n\overline{w}\tau + \overline{B_n}\sin n\overline{w}\tau\right) \tag{3.22}$$

Notice that this procedure returns 7 non-dimensional groups that, in addition to f_0, which was already introduced in equation (3.8), govern the problem

$$\overline{\omega} = \omega\sqrt{\frac{\rho B^2}{C_{\mathrm{N10}}}} \qquad \kappa = \frac{\mu}{B\sqrt{\rho\, C}} \qquad \overline{\rho} = \frac{\rho_f}{\rho}$$

$$\overline{P_m} = \frac{P_m}{C_{\mathrm{N10}}} \qquad \overline{p}_\infty = \frac{p_\infty}{C_{\mathrm{N10}}} \qquad \overline{\psi}(\lambda) = \frac{\psi(\lambda)}{C_{\mathrm{N10}}}$$

$$\overline{A_i} = \frac{A_i}{C_{\mathrm{N10}}} \qquad \overline{B_i} = \frac{B_i}{C_{\mathrm{N10}}} \quad \text{for} \quad i = 1, 2, 3, 4, 5$$

where $\overline{\psi}(\lambda) = \psi(\lambda)/C_{\mathrm{N10}}$ is the non-dimensional strain energy function, κ defines the ratio between the characteristic time scales (speed of stress waves) of CSF and aneurysm's wall, $\overline{\rho}$ is the ratio between CSF and aneurysm's wall densities and $\overline{\omega}$ the dimensionless fundamental angular frequency. Moreover, P_m is the dimensionless mean pressure applied in the inner surface of the aneurysm and p_∞ is the dimensionless remote pressure, which together may be found as $\overline{\Delta P} = \overline{P_a}(\tau) - \overline{p}_\infty$ i.e., the pressure difference between the blood flow and the far field in the CSF. Notice that the parameter C_{N10} is used to non-dimensionalize both constitutive models since to be compared they have to be subjected to the same conditions. $\overline{A_i}$ and $\overline{B_i}$ are just the factors determining the behaviour of the pulsatile flow.

3.4 Balance of Mechanical Energy

For further characterization of the problem energies are calculated. So if equation (3.21) is multiplied by $2\lambda_b^2$,

$$\begin{aligned} 2\lambda_b^2\,\overline{\Delta P} = \overline{\rho}\,\frac{\mathrm{d}}{\mathrm{d}\lambda_b}\left(\lambda_b^3\dot{\lambda_b}^2\right) + 8\,\kappa\,\lambda_b\dot{\lambda_b} + \\ + 2\lambda_b^2\int_{\lambda_b}^{\left(\frac{\lambda_b^3+f_0-1}{f_0}\right)^{1/3}} \frac{\overline{W'(\lambda)}}{\lambda^3-1}\,\mathrm{d}\lambda - \frac{\mathrm{d}}{\mathrm{d}\lambda_b}\left(\left(1-\frac{\lambda_b}{(\lambda_b^3+f_0-1)^{1/3}}\right)\lambda_b^3\dot{\lambda_b}^2\right) \end{aligned} \tag{3.23}$$

Now, equation (3.23) is integrated over λ between $\lambda_b(0)$ and $\lambda_{b_{max}}$ and $\lambda_b(0) = 1$ and $\dot{\lambda_b}(0) = 0$ considered as initial conditions (the aneurysm is initially at rest and unstretched). Then, by performing a change of variable where $\lambda_b = \zeta$ and the integration limits become 1 and λ_b the final expression[4] for the energy terms is:

$$\begin{aligned} 2\overline{\Delta P}\frac{\lambda_b^3-1}{3} = \overline{\rho}\lambda_b^3\dot{\lambda}_b^2 + 8\kappa\int_1^{\lambda_b}\lambda_b\dot{\lambda_b}\mathrm{d}\zeta + \\ + 2\int_1^{\lambda_b}\lambda_b^2\int_{\lambda_b}^{\left(\frac{\lambda_b^3+f_0-1}{f_0}\right)^{1/3}}\frac{\overline{\psi}'(\lambda)}{\lambda_b^3-1}\,\mathrm{d}\lambda\,\mathrm{d}\zeta - \lambda_b^3\dot{\lambda_b}^2\left(1-\frac{\lambda_b}{(\lambda_b^3+f_0-1)^{1/3}}\right) \end{aligned} \tag{3.24}$$

[4]For the complete derivation of equation (3.24), see appendix A.4

From the previous equation, it can be observed that the balance of mechanical energy is

$$\overline{\Pi_e} = \overline{\Pi_s} + \overline{\mathcal{K}_s} + \overline{\mathcal{K}_f} + \overline{\mathcal{D}_f} \tag{3.25}$$

So, comparing equation (3.24) and (3.25) and performing a change of variable to integrate equation (3.24) along time, considering that $\mathrm{d}\lambda_b = \dot{\lambda_b}\mathrm{d}\xi$, the final expressions for the energies governing the problem result as:

$$\overline{\Pi_e} = 2\overline{AP}\frac{\lambda_b^3 - 1}{3} \tag{3.26a}$$

$$\overline{\Pi_s} = 2\int_0^\tau \lambda_b^2\dot{\lambda}_b \int_{\lambda_b}^{\left(\frac{\lambda_b^3+f_0-1}{f_0}\right)^{1/3}} \frac{\overline{\psi}'(\lambda)}{\lambda_b^3 - 1}\,\mathrm{d}\lambda\,\mathrm{d}\xi \tag{3.26b}$$

$$\overline{\mathcal{K}_s} = -\lambda_b^3\dot{\lambda_b}^2\left(1 - \frac{\lambda_b}{(\lambda_b^3 + f_0 - 1)^{1/3}}\right) \tag{3.26c}$$

$$\overline{\mathcal{K}_f} = \overline{\rho}\lambda_b^3\dot{\lambda}_b^2 \tag{3.26d}$$

$$\overline{\mathcal{D}_f} = 8\kappa\int_0^\tau \lambda_b\dot{\lambda}_b^2\mathrm{d}\xi \tag{3.26e}$$

where $\overline{\Pi_e}$ is the work done by the external forces, $\overline{\Pi_s}$ the elastic energy stored by the aneurysm's wall, $\overline{\mathcal{K}_s}$ the kinetic energy of the aneurysm, $\overline{\mathcal{K}_f}$ the kinetic energy of the CSF and $\overline{\mathcal{D}_f}$ the viscous dissipation given by the surrounding CSF.

3.5 Analitical Solution

For the case $\kappa = 0$ (i.e. non-viscous Newtonian CSF), equation (3.24) turns into a single variable equation that can be solved analytically. So without the viscous depending term and solving for the stretch rate from equation (3.24), it results that:

$$\dot{\lambda_b} = \left(\frac{2\overline{AP}\frac{\lambda_b^3-1}{3} - 2\int_0^\tau \lambda_b^2\dot{\lambda}_b \int_{\lambda_b}^{\left(\frac{\lambda_b^3+f_0-1}{f_0}\right)^{1/3}} \frac{\overline{\psi}'(\lambda)}{\lambda_b^3-1}\,d\lambda\,d\xi}{\lambda_b^3\left(\overline{\rho} - 1 + \frac{\lambda_b}{(\lambda^2+f_o-1)^{\frac{1}{3}}}\right)}\right)^{\frac{1}{2}} \tag{3.27}$$

The final expression of the stretch rate $\dot{\lambda_b}$ depending in the stretch λ_b in terms of the total potential energy is presented below:

$$\dot{\lambda_b}(\lambda_b) = \left(\frac{\overline{\Pi_e} - \overline{\Pi_s}}{\lambda_b^3 \left(\overline{\rho} - 1 + \frac{\lambda_b}{(\lambda^2 + f_o - 1)^{\frac{1}{3}}} \right)} \right)^{\frac{1}{2}} \tag{3.28}$$

3.6 Numerical Solution

Finally, in order to obtain λ_b in any conditions, equation (3.21) is reduced to a system of two first-order differential equations. Being $z_1 = \lambda_b$ and $z_2 = \dot{\lambda_b}$

$$z_2 = \dot{z_1} \tag{3.29}$$

$$\dot{z_2} = \frac{\overline{\Delta P} - \int_{z_1}^{\left(\frac{z_1^3 + f_0 - 1}{f_0}\right)^{1/3}} \frac{\overline{\psi}'(\lambda)}{\lambda^3 - 1}\, d\lambda - 4\kappa \frac{z_2}{z_1} + z_2^2 \left(\frac{3}{2} + \frac{z_1^4}{2\left(z_1^3 + f_0 - 1\right)^{4/3}} - \frac{2z_1}{\left(z_1^3 - f_0 - 1\right)^{1/3}} - \frac{3}{2}\overline{\rho} \right)}{z_1 \left(\overline{\rho} + \frac{z_1}{\left(z_1^3 + f_0 - 1\right)^{1/3}} - 1 \right)} \tag{3.30}$$

they are solved numerically using a fourth-order Runge-Kutta method available in MATLAB for stiff differential equations. Recall that the motion of every material point along the aneurysm's wall is determined once λ_b is known.

Chapter 4

Constitutive Modelling

A constitutive model is a mathematical description of how materials respond to various loadings [41]. It is calculated by fitting all the data obtained after performing different tests to the desired material. Then, the isotropic elastic properties of materials are described in terms of a strain-energy function [21] such as:

$$\psi = f\left(I_1, I_2, I_3\right)$$

where I_1, I_2 and I_3 are the three invariants of the Cauchy-Green deformation tensor. In terms of the principal stretches they are:

$$I_1 = \lambda_1^2 + \lambda_2^2 + \lambda_3^2$$
$$I_2 = \lambda_1^2\lambda_2^2 + \lambda_2^2\lambda_3^2 + \lambda_3^2\lambda_1^2$$
$$I_3 = \lambda_1^2\lambda_2^2\lambda_3^2$$

In this work, two different strain energy functions are used to describe the mechanical behaviour of the aneurysmal wall. They both respond to the following polynomial form:

$$\psi = \sum_{i,j=0}^{N} C_{ij}(I_1 - 3)^i(I_2 - 3)^j \tag{4.2}$$

where C_{ij} are empirically determined material parameters and I_1, I_2 are the first and second invariants of the left Cauchy-Green strain tensor, respectively. Namely, the so-called Neo-Hookean and 3-parameters Mooney-Rivlin models are used. These two

models probably are the ones better known and more used [21] but also they fit quite well the data coming from aneurysms [45]. The aim of this work was to select two constitutive models calibrated for biological parameters. Furthermore, they have been selected so that one of them will bifurcate at some point whereas the other will never bifurcate (later deeply explained in chapter 5). So finally, the resulting constitutive models are:

- Neo-Hookean model

$$\psi = C_{\mathrm{N10}}(I_1 - 3) \tag{4.3}$$

- 3-parameters Mooney-Rivlin model

$$\psi = C_{\mathrm{M10}}(I_1 - 3) + C_{\mathrm{M01}}(I_2 - 3) + C_{\mathrm{M11}}(I_1 - 3)(I_2 - 3) \tag{4.4}$$

The 3-parameter Mooney-Rivlin model was calibrated by Costalat et al. [13] using experimental results obtained from 16 intracranial saccular aneurysms tested in uniaxial tension under physiological conditions. The resulting parameters values are: $C_{\mathrm{M10}} = 0.19$ MPa, $C_{\mathrm{M01}} = 0.024$ MPa and $C_{\mathrm{M11}} = 7.87$ MPa. For the Neo-Hookean model, which is a reduction of the Mooney-Rivlin model, $C_{\mathrm{N10}} = 0.214$ MPa has been taken to ensure that Neo-Hookean and Mooney-Rivlin models provide the same initial shear modulus. The comparison between these two models developed in chapter 5 brings to light the key role played by the mechanical behaviour of the aneurysmal wall in the dynamic response of the aneurysm.

Chapter 5

Results

The following chapter analyzes how different biological parameters affect the behaviour of the aneurysm. In section 5.1, the most basic model where the internal applied pressure is constant and there is no viscosity contribution from the surrounding cerebrospinal fluid is considered. The model is tested for different values of the dimensionless constant internal pressure, the dimensionless thickness and the dimensionless density. From this analysis it is concluded how these parameters affect the possible rupture of the aneurysm's wall.

In section 5.2, the viscosity given by the external surrounding fluid is incorporated to the model. It is explored how the aneurysm's growth is affected when applying a viscosity value similar to that one of the CSF in humans and which viscosity will be necessary to attenuate the oscillation of the aneurysm wall.

Finally, in section 5.3 is included a pulsatile pressure applied to the internal wall of the aneurysm. Living beings are characterised for having a pulsatile blood flow circulating along the body and here it is explored how it affects the development of the aneurysm and if it has a relevant role on its possible rupture.

5.1 Aneurysm's Model: Non-Viscous CSF and Constant Internal Pressure

The different affecting parameters are explored to the limit case where the aneurysm bifurcates (it is assumed that at the point of the bifurcation the aneurysm will break). All of them are presented in comparison with the reference case, considering the reference pressure, density and radius as those ones presented in the works of Costalat et al. and Shah and Humphrey, where $P_m = 67.5\,\text{mmHg}$, $p_\infty = 3\,\text{mmHg}$, $\rho = 1050\,\text{kg/m}^3$,

$\rho_f = 1000\,\mathrm{kg/m^3}$ [32, 48] and $A = 4.3\,\mathrm{mm}$ and $B = 4.67\,\mathrm{mm}$ [13]. Those values result in the following dimensionless parameters:

$$\overline{\Delta P} = 0.0391 \qquad \overline{\rho} = 0.9524 \qquad f_0 = 0.7806$$

which are the ones varied during the parametric analysis. Remember that in this section there is no viscosity contribution from the external surrounding fluid and that the internal pressure is constant.

In all the cases, the two constitutive models analyzed in this work are presented together, comparing their different features. The models, as explained in section 4, are the Neo-Hookean and the Mooney-Rivlin with 3 parameters. Since the problem has been develop in a 3 dimensional framework, every model of order 3 or smaller will bifurcate at some point whereas those with order higher than 3, won't bifurcate. In this case, the Neo-Hookean model, who is an O(3) constitutive model, will always bifurcate at some point, as checked later in this section. In contrast, Mooney-Rivlin for three parameters won't reach the bifurcation point at any time since it is an O(4) model.

In this work the limit cases when the aneurysm model bifurcates are explored in order to see whether the bifurcation point coincides with an achievable biological value or not. Furthermore, the study of those cases allow to set at which conditions the intracranial saccular aneurysm, under the selected constitutive model, will break.

So now starts the analysis of the model given there is a constant internal pressure and zero viscous CSF contribution. For the case of variable pressure values, figure 5.1 shows three different cases: the first one, represented with a continuous blue line and marked in the legend with and asterisk (*), represents the reference case, for which none of the parameters presented above have been varied, the second one, dashed orange line, is the case associated with one of the first values at which the bifurcation occurs and the third one, dotted green line, corresponds with a case at which the models bifurcates from the very beginning. Notice that this scheme is the same in figure 5.2.

When no bifurcation occurs, the total potential energy (graphs 5.1a and 5.1b for both Neo-Hookean and Mooney-Rivlin models) remains positive. Also notice that when there is no bifurcation, the total potential energy varies when changing the parameters, meaning that the distribution of energy is shifting between the external forces and the solid's wall. However, when a bifurcation occurs and the aneurysm stops oscillating, the potential energy passes to be dominated by the energy provided by the solid, which diverges to negative values. Additionally, in the case of bifurcation, the stretch ratio tends to a constant value, as it is shown in graph 5.1c.

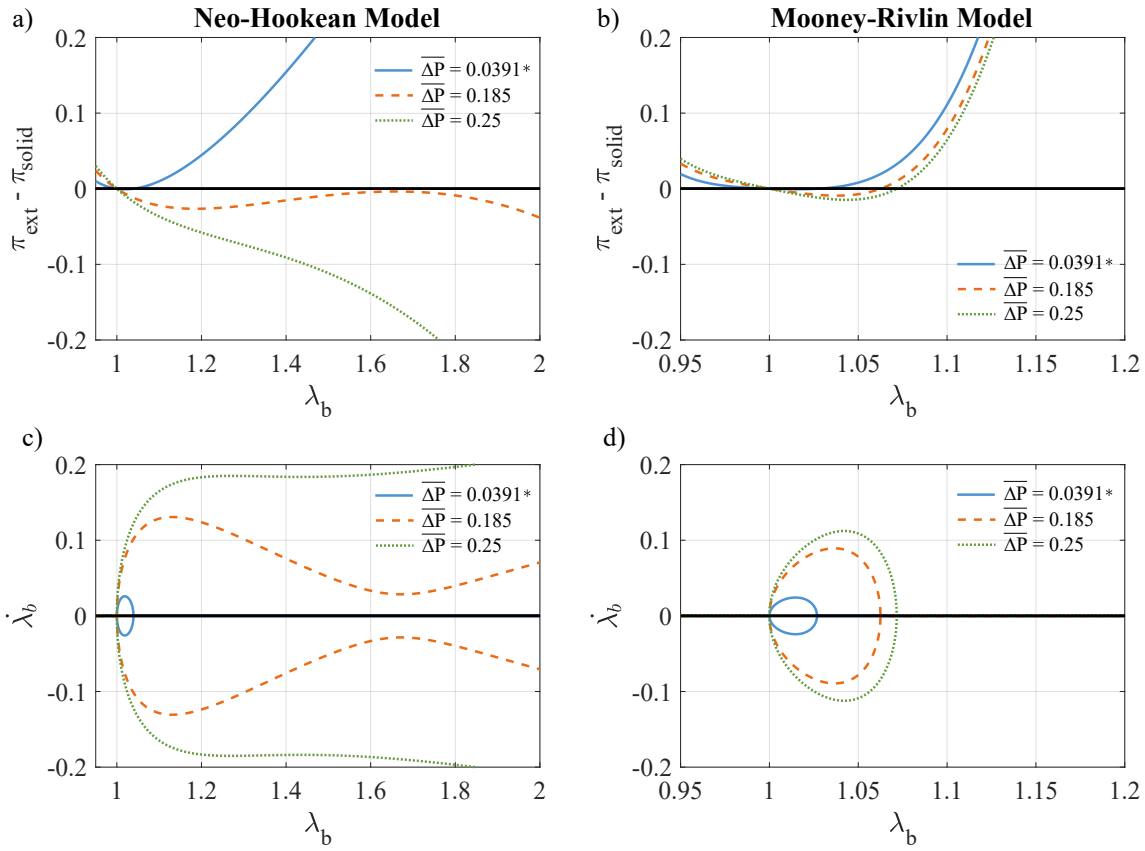

Figure 5.1: Comparison of the aneurysm's model subjected to two different constitutive models, Neo-Hookean, a) and c), and Mooney-Rivlin, b) and d), for various dimensionless pressure at $f_0 = 0.7806$, $\overline{\rho} = 0.9524$ and $\kappa = 0$. a) and b) corresponds with the variation of potential energy for the different models whereas c) and d) represent the phase diagrams resulted form each model.

It is shown that no bifurcation occurs at biological values (there is no bifurcation at the reference case) neither for the Neo-Hookean model neither for the Mooney-Rivlin of three parameters. Maintaining the thickness and density parameters constant but varying the dimensionless internal constant pressure from 0.0391 (dimensionless reference pressure) to 0.1850, a bifurcation occurs in the Neo-Hookean model. Thus, for any value higher than 0.1850 in the Neo-Hookean model a bifurcation will occur and the aneurysm's wall will break.

However, according to the data provided by Williams et al. [58], just adults with a severe type of hypertension will achieve values of pressure equal or higher to 180 mmHg, which corresponds with a dimensionless pressure of 0.1121. Although this value is not

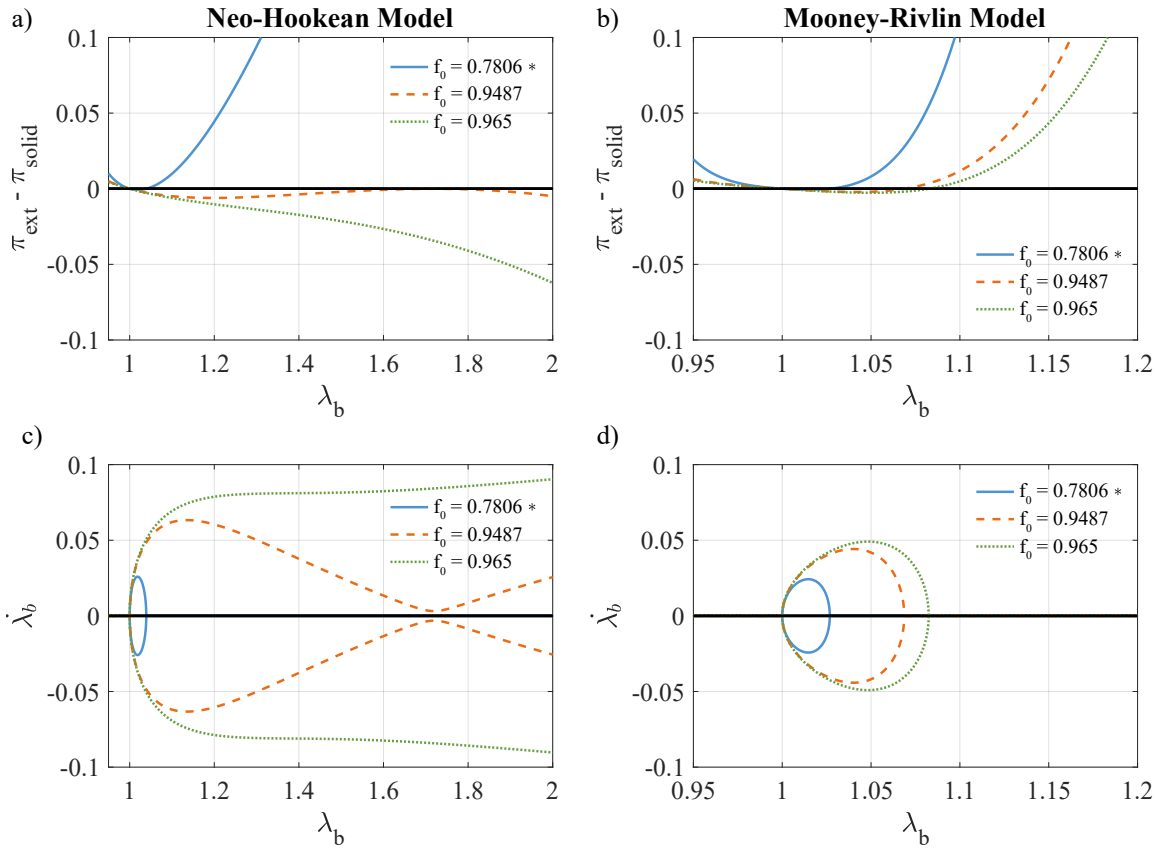

Figure 5.2: Comparison of the aneurysm's model subjected to two different constitutive models, Neo-Hookean, a) and c), and Mooney-Rivlin, b) and d), for various dimensionless radius at $\overline{\Delta P} = 0.0391$, $\overline{\rho} = 0.9524$, $\kappa = 0$. a) and b) correspond with the variation of potential energy for the different models whereas c) and d) represent the phase diagrams resulted form each model.

enough for the bifurcation to occur and is relatively far from the pressure needed (about 296 mmHg) it seems that the influence of pressure is relevant enough and it should be explored for other and more accurate constitutive models.

In contrast, Mooney-Rivlin's model behaves in a different manner. It does not bifurcate for the same values as Neo-Hookean. Furthermore, much higher values have been explored (up to $\overline{\Delta P} = 1000$) but no bifurcation appears. This phenomena occurs due to the relation between the order of the constitutive model and the dimension in which the problem is formulated, demonstrating that the final problem highly depends on the constitutive model.

Now, continuing with figure 5.2, the variations with respect to the internal and external radius are explored. As before, three different situations appear, one with the reference case and another two exploring the bifurcations points. So, for the case of Neo-Hookean model, the bifurcations appears at a value of $f_0 = 0.9478$, far enough from the reference value ($f_0 = 0.7806$) at physiological conditions. To check this fact, a further point is explored ($f_0 = 0.9650$) to confirm the behaviour of the model for values of the dimensionless thickness equal or greater than 0.9478. As it is possible to see in this figure, the curve bifurcated at the very beginning of the cycle. Then, as expected, no bifurcation occurs at any of the presented points for the case of the Mooney-Rivlin. It has been tested for values of $f_0 \longrightarrow 1$, resulting in no bifurcation.

Notice that having the dimensionless parameter $f_0 \sim 1$, means having a really thin aneurysm's wall where the internal and external radius are almost the same and at this case the membrane theory (section 2.2) could be assumed. Moreover, in this simulation having a value greater than 1 has no sense since it would mean having an internal radius grater than the external, what is physically impossible.

As occurred when changing the pressure values, the total potential energy varies between the different cases, ending with negative values when the model bifurcates. For the cases no bifurcation occurs, the potential energy experiments a variation and the maximum stretch achieved during each oscillation is incremented, as well as the velocity of the oscillation.

When talking about biological values there is a broad range of possibilities. This project, following the work of Costalat et al. [13], has considered the thick-walled theory to compute the model. However, the thickness of aneurysms vary considerably, finding in literature small aneurysms with a thickness between 0.02 mm [10, 24] and 0.08 mm [27], whose models could be calculated assuming the membrane's theory, and others with larger thickness as 0.375mm [56] or even 0.51mm [31]). By this reason, not assuming the membrane's theory allow more accurate results when defining the fate of the aneurysm. Small differences in thickness will be registered and considered for thin aneurysms that otherwise would be considered to have the same one and also it will be valid for aneurysms with a thicker wall.

Figure 5.2c shows that at reference conditions no aneurysm will break. However, for the thinner intracranial aneurysms there will a limit thickness for which a bifurcation will occur and consequently, the rupture of the aneurysm. So aneurysms with a thickness around 0.08 mm or smaller, whose $f_0 \sim 0.92590$ or higher, will break given the rest of the parameters remain constant as occur in the reference case. Nevertheless, the thicker ones will not rupture.

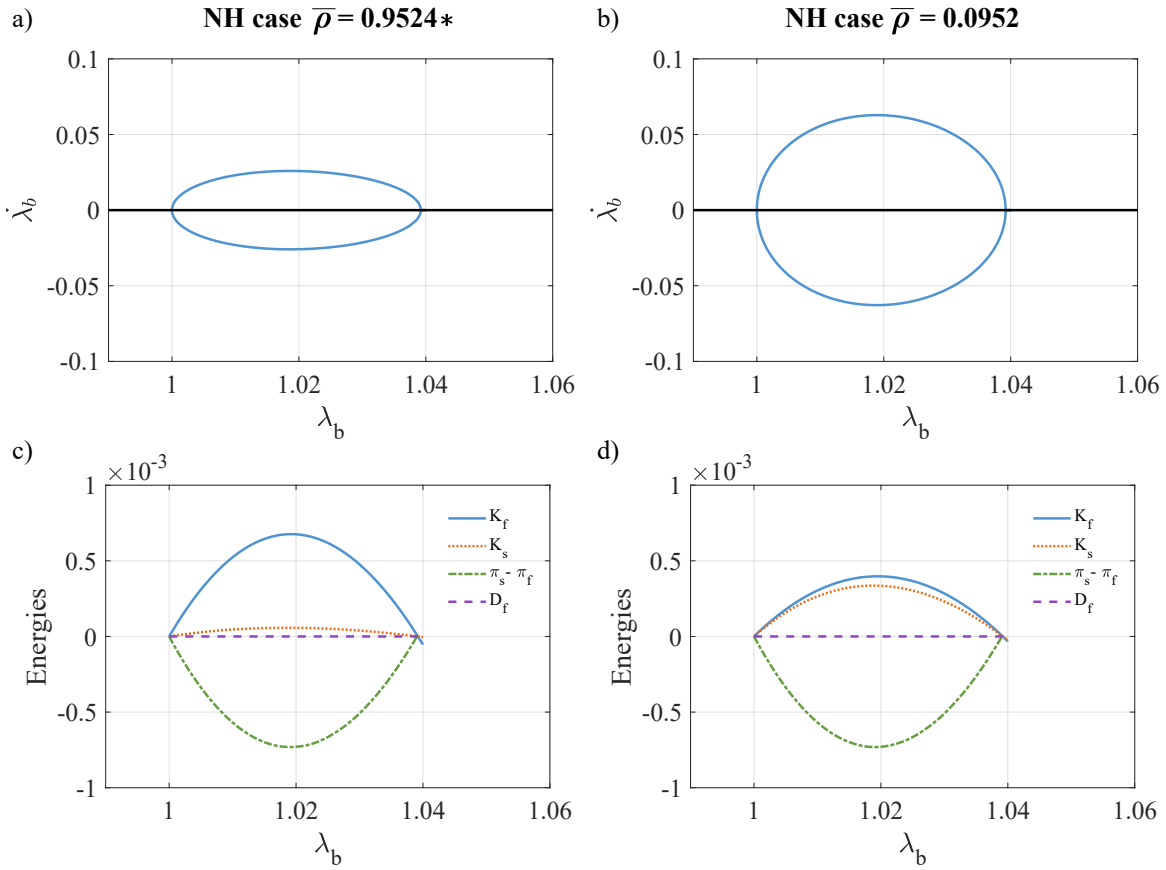

Figure 5.3: Analysis of the different energies for the Neo-Hookean model for dimensionless densities, AP = 0.0391, $f_0 = 0.7806$, $\kappa = 0$ and constant internal pressure, being Π_e the work done by the external forces, Π_s the elastic energy stored by the aneurysm's wall, $\mathcal{K}_s$ the kinetic energy of the aneurysm, $\mathcal{K}_f$ the kinetic energy of the CSF and $\mathcal{D}_f$ the energy dissipated by the CSF, respectively. a) is the variation of energies for $\overline{\rho} = 0.9524$, b) the variation for $\overline{\rho} = 0.0952$, c) the phase diagram in reference case and d) the phase diagram for $\overline{\rho} = 0.0952$.

Finally, the last parameter analyzed for the case of constant internal pressure and no viscosity contribution is the dimensionless density. In this case no bifurcation occurs neither in the Neo-Hookean model neither in the Mooney-Rivlin for three parameters. For the case of the reference viscosity $\overline{\rho} = 0.9524$ it is shown a determined amplitude for the oscillation of the aneurysm's wall. Depending on which density has more influence, the velocity of the oscillation of the aneurysm's wall will be bigger or smaller but the maximum and minimum stretch will remain constant along different densities. By this way, by increasing the dimensionless density up to $\overline{\rho} = 2.0000$ the velocity of the

oscillation decreases whereas by decreasing it to $\overline{\rho} = 0.0952$, the velocity increases much more. Thereby, an increase in the dimensionless density results in a decrease in the velocity of vibration of the aneurysm's wall while a decrease in the dimensionless density, into an increase in the velocity of the oscillation (see figure 5.3a and 5.3d).

In this case the variation of potential energy has no interest at all since the values of the maximum and minimum stretches are the same and the model never bifurcates. This is translated into a non-dependant potential energy in the density of the solid and the fluid. However, the potential energy is not the only one governing the problem, so an analysis of the different energies affecting the deformation of aneurysm's wall is presented in figures 5.3a and 5.3b.

First of all notice that the contribution due to the dimensionless fluids viscosity $\mathcal{D}_f$ (dashed purple plot) is always 0, which has sense since this sections is studied without the contribution of the external fluid's viscosity, i.e. $\kappa = 0$. Then, the potential energy $\overline{\Pi}_s - \overline{\Pi}_f$ (dashed-dotted green plot) is always keep constant and shows no variation with respect to the variations in the dimensionless density, as explained before. Therefore, the total contribution from the work exerted by the external forces and the elastic energy of the aneurysm's wall is maintained constant since it is a conservative system and no energy is dissipated. Finally, it is possible to appreciate that the variations in the dimensionless density are dominated by the total kinetic energy. For higher values of the density, as the reference one, the total kinetic energy of the cerebrospinal fluid $\mathcal{K}_f$ (blue line) almost totally overcomes with the total kinetic energy. However, as the dimensionless density is diminished the kinetic energy of the solid $\mathcal{K}_s$ (dotted orange graph) plays a major contribution on the total kinetic energy of the system. Therefore, the lower the dimensionless density, the higher the contribution exerted by the kinetic energy of the solid and therefore, for sufficiently small values of the dimensionless density, the contribution to the model of the external surrounding cerebrospinal fluid will be almost none.

From section 3.3 it is known that $\overline{\rho} = \frac{\rho_f}{\rho}$, being ρ_f the density of the fluid and ρ the density of the aneurysm's wall. Therefore, the above results has sense since the lower the dimensionless density is, the higher is the contribution of the solid's density and therefore, the kinetic energy exerted by the solid. Vice versa, the higher the value of the dimensionless density, the higher the contribution of the external fluid's density and consequently, the higher the kinetic energy of the CSF.

5.2 Aneurysm's Model: Viscous CSF and Constant Internal Pressure

In this subsection, the viscosity of the external fluid is included into the model ($\kappa \neq 0$). Remember that κ is not exactly the dimensionless viscosity but the ratio between the time scales of CSF and the aneurysm's wall i.e.,

$$\kappa = \frac{\mu}{B\sqrt{\rho C_{\mathrm{N10}}}}$$

However, since the rest of the parameters are going to be maintained constant in this analysis, the variation of κ means a variation in the viscosity of the CSF. Therefore, this subsection is going to analyze what is the real role of the viscosity coming from the CSF and if the dissipation of energy considerably augments. Hence, its behaviour over the aneurysm's wall is going to be observed as well as its real contribution in the bifurcation of the model.

In a first attempt, the model has been computed with the viscosity given by Shat et al. [48]. Using $\kappa = 1.8 \cdot 10^{-6}$, which corresponds with a viscosity value of $1.26 \cdot 10^{-4}$ Ns/m^2

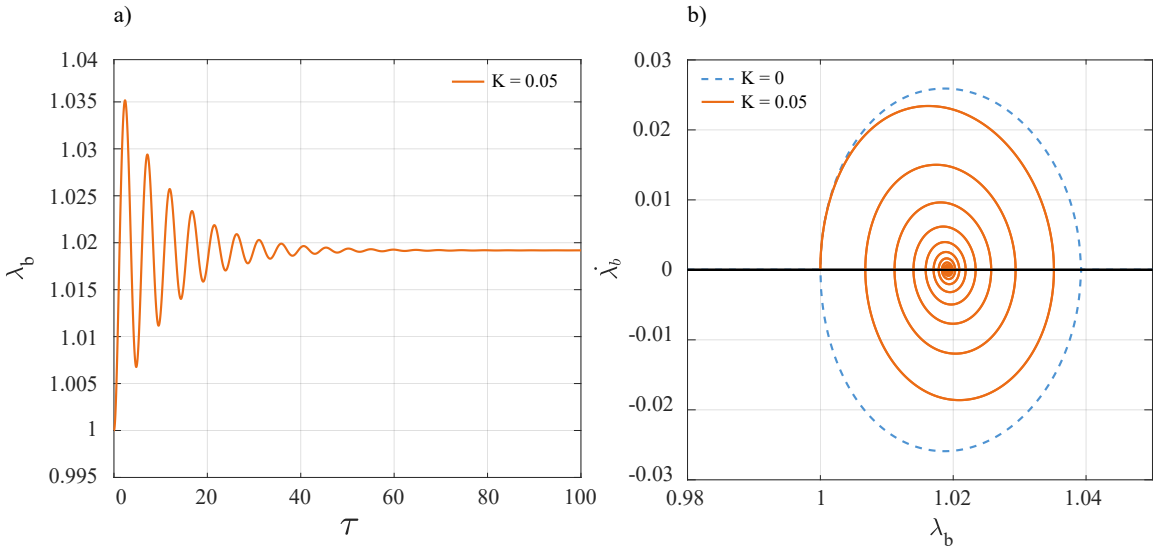

Figure 5.4: Aneurysm's model at reference conditions ($\overline{\Delta P} = 0.0391$, $\overline{\rho} = 0.9524$ and $f_0 = 0.7806$) with a viscosity of $\kappa = 0.5$ and a constant internal pressure for the Neo-Hookean model. Graph a) shows how the stretch evolves over time and graph b), the phase diagram.

no differences were found with respect the reference conditions at which $\kappa = 0$. The viscosity given by the fluid is so small that is almost negligible. Hence, it results into a system that is mainly elastic where almost no dissipation of energy is appreciated and no cushioning of the oscillation of the aneurysm's wall appears.

Consequently, a further analysis is performed with a viscosity higher enough to study the limit case at which this parameter plays a major role in the attenuation of the oscillation. When exploring the possible values for κ, it was found that the one needed for the viscosity to govern the attenuation of the aneurysm was $\kappa = 0.05$, that corresponds with a viscosity of 3.5002 Ns/m^2, which is much more orders of magnitude higher than the biological one. Although some authors have reported variations in the viscosity of the CSF [6], none of them have reported such a big value. From this data it can be concluded that the contribution of the viscosity coming from the CSF in reference conditions is not relevant to the problem. Nevertheless, since κ is not a single parameter dependent, it is going to be studied the limit case to understand how it affects the dynamic behaviour of the aneurysm and which values are required for this behaviour to occur.

Figure 5.4a shows the variation of the stretch along the dimensionless time τ. It can be easily deduced from the graph that the aneurysm is oscillating at time $\tau = 0$ but that the amplitude of the oscillation decreases in each period. At the end, the oscillations dies in an attractor point [1] that corresponds with an stretch value of $\lambda_b \sim 1.02$. From this value is concluded that the final state of the aneurysm is a deformed non-oscillating one and that the aneurysm do not undergo any bifurcation. Figure 5.4b represents the phase diagram of the aneurysm's model with $\kappa = 0$ under reference conditions (dashed blue line) and $\kappa = 0.05$ (continuous orange line). As observed in graph a), the viscous contribution is sufficiently high to decrease the amplitude of the oscillation to none, dissipating all the energy over the system and leading to a deformed static aneurysm.

5.3 Aneurysm's Model: Viscous CSF and Pulsatile Internal Pressure

Finally, an internal pulsatile flow is included into the model. This section is oriented to understand which is the behaviour of aneurysms under a pulsatile internal pressure, so the different parameters affecting the model are not going to be varied. Since κ at reference conditions has almost no contribution to the model, it is increased to $\kappa = 0.05$ for a better illustration of energy dissipation by the CSF.

[1] An attractor points corresponds with the stretch value at which an oscillation stops.

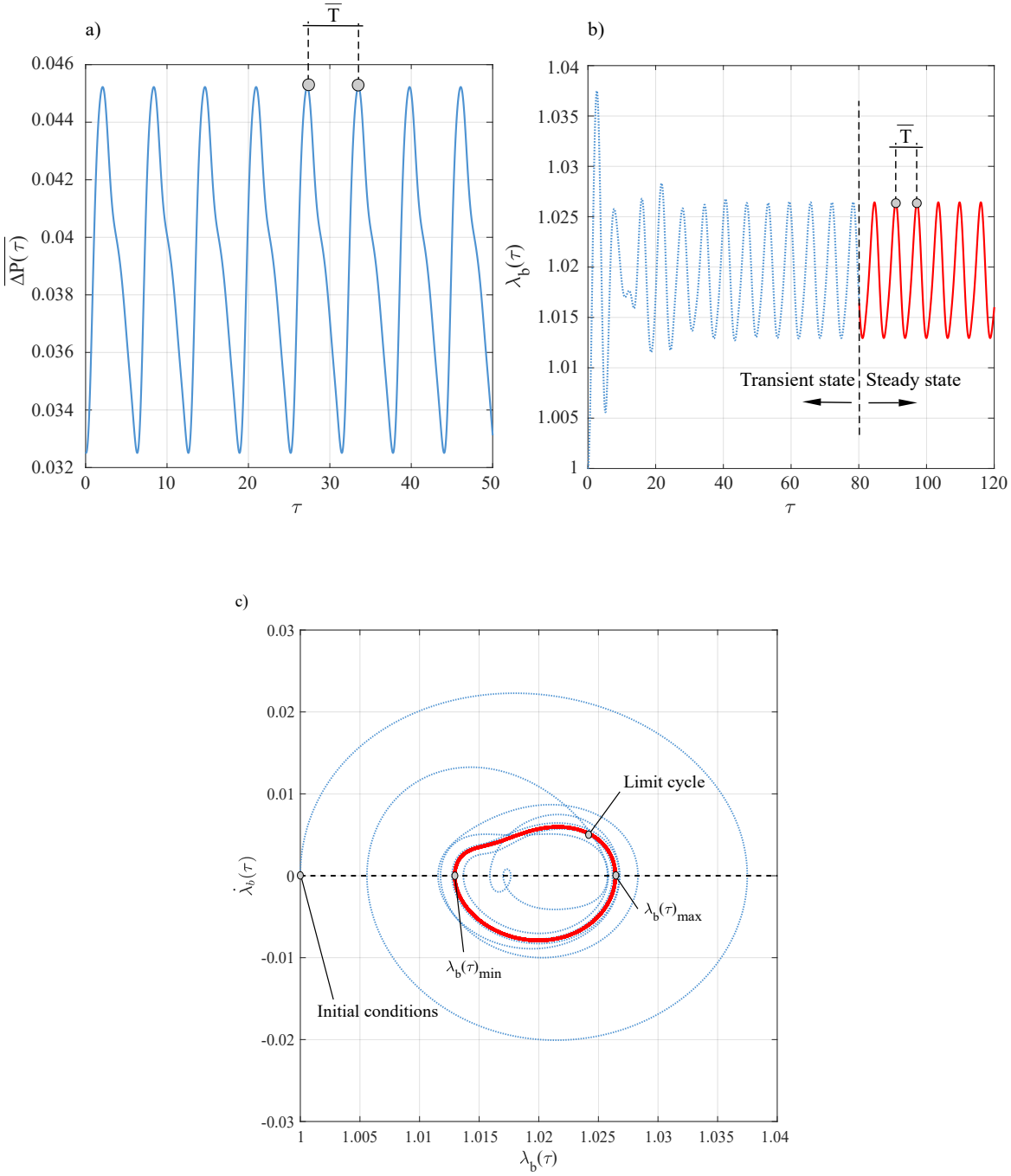

Figure 5.5: Effect of a variable internal pressure in the aneurysm's model at $f_0 = 0.7806$, $\overline{\rho} = 0.9524$, $\kappa = 0.05$ and $\overline{\omega} = 1$. in graph a), the variation of the dimensionless pressure $\overline{AP}$ versus the loading time τ, in b), the circumferential stretch in the outer surface of the aneurysm λ_b versus the loading time τ and in c), the circumferential stretch rate $\dot{\lambda}_b$ versus the circumferential stretch λ_b in the outer surface of the aneurysm (phase diagram).

Notice that when the reference value is employed, there will be a point at which a limit cycle will be achieved. However, the required time for reaching this state will be much longer. So as before, the aneurysm is assumed to be initially unstretched and at rest and the applied frequency will be $\overline{\omega} = 1$ since it is near to the frequency of resonance of the solid structure, $\overline{\omega} \simeq 1.16$.

Therefore, figure 5.5a shows the dependence of the applied pressure with time. $\overline{T}$ corresponds with the period given by dimensionless frequency, which is determined by the time elapsed between two consecutive peaks. Then in figure 5.5b, the circumferential stretch in the outer surface of the aneurysm evolves over the dimensionless loading time. Two different states are distinguished: the transient state (dotted blue line) and the steady state (solid red line). The transient state last until $\tau \simeq 80$ and is characterised by the evolution of λ_b before it stabilises in time. The circumferential stretch undergoes a brief variation in the amplitude of its oscillation until it stabilises, behaviour caused by the energy dissipation produced by the CSF. Then, during the steady state, at any dimensionless time $\tau \geq 80$, the aneurysm's wall will undergo the same oscillation corresponding with the stabilisation of the circumferential stretch over time. This will be the periodic response of the aneurysm.

Finally, figure 5.5c shows the phase diagram corresponding to the outer surface of the aneurysm. In this case the dashed line also corresponds with the transient response whereas the solid red one, with the steady state. The transient response is associated with a gradual reduction in the velocity and amplitude of the oscillations until it reaches the steady state, where the motion of the oscillations becomes periodic and follow the non-symmetric geometry illustrated in the limit cycle. The limit cycle (solid red line) results from the balance between the work of the applied pressure and the energy dissipated by the CSF and corresponds with the cycle in the phase diagram around which the oscillation of the wall of the aneurysm stabilizes.

Chapter 6

Conclusions and Future Work

6.1 Conclusions

3% of the worldwide population is affected by intracranial aneurysms. Among them, the most common ones are the intracranial saccular aneurysms. Their rupture leads to subarachnoid haemorrhages, which in most cases results in brain damage or death.

There are many factors affecting the growth and rupture of intracranial aneurysms. They can vary depending on where they are located, their geometry and their growth, how the flow interacts with the aneurysm's wall, if an individual has a genetic disease or not or even it he smoke or have hypertension and his sex and age. All those factors have been proved to influence the rupture of the aneurysms; however, when the physicians are about to decide the treatment of the aneurysm, the most important parameter to consider is the size.

Therefore, there is a need on physically understanding how the aneurysm evolve considering all the aforementioned parameters. By this reason, this work has developed a mathematical model of an idealized intracranial saccular aneurysm in an attempt to understand how the aneurysm's wall behaves when modeled with different constitutive formulations, which include the characteristics of the aneurysm's wall.

In this project the formulation developed by Shah and Humphrey [48] has been extended to a 3D framework to model the dynamic behaviour of idealized intracranial saccular aneurysms subjected to pulsatile blood flow and surrounded by the cerebrospinal fluid. The need for a 3D formulation arises from the experimental measurements of Suzuki and Ohara [51], MacDonald et al. [34] and Costalat et al. [13] who provided evidences of saccular aneurysms with ratios between wall thickness and inner radius larger that 0.1.

So, starting from an infinitesimal spherical element and setting the equilibrium, the 3D framework is developed. In addition, for a further understanding of the problem, the different governing energies are also obtained. The work is divided in an analysis of three different situations: firstly the mathematical model is presented with an internal constant pressure and with no viscous contribution by the external surrounding fluid, secondly, the viscosity is included and finally, an internal pulsatile pressure that simulates human's blood flow. In the first case, two different constitutive models (Neo-Hookean and Mooney-Rivlin for three parameters) are compared. However in the following sections, just the Neo-Hookean is consider for the computations. Furthermore, in the first case a parametric analysis is performed in order to clarify which is the effect of some biological parameters as the pressure, thickness and density. The use of Mooney-Rivlin model shows that the mathematical model is strongly affected by the constitutive model and the that the results are highly dependant on it.

For the case of constant internal pressure and no external fluid viscosity, the dimensionless pressure, the dimensionless ratio of the radius and the dimensionless density have been analyzed. For the case of constant pressure it has been found that the pressure needed for a bifurcation to occur is out of the range of the biological ones. In the Neo-Hookean model a bifurcation will occur approximately at a $P_m = 296\,\text{mmHg}$. However, since this value of pressure is not so far from the highest achieved by humans in the extreme situations and the model is highly dependent on the constitutive model, it is possible that other constitutive models may bifurcate at a lower pressure value.

When analyzing the effect of the dimensionless radius, it was found that some of the biological sizes of the wall aneurysm lay between the bifurcation range. But more important that the average size, it is the thickness of the wall. For a Neo-Hookean model a bifurcation occurs at $f_0 = 0.9478$, which means that aneurysms with thickness around 0.08 mm or smaller will break. Of course, it is highly dependent on the constitutive model, which includes all the parameters influencing the behaviour of the aneurysm.

Finally, the last parameter analyzed was the dimensionless density, which has no influence in the rupture of the aneurysm (no bifurcation occurs when changing the density of the solid and the fluid but it influences the velocity of the oscillation of the aneurysm's wall). However, from this analysis it is concluded that as the density of the fluid is incremented over the solids one, the kinetic energy governing the problem will be that one of the fluid and vice versa.

When including the viscosity exerted by the CSF, resulted that it is so small value that it not contributes to the dissipation of energy neither to the reduction of the oscillation of the aneurysm's wall. However, notice that the parameter κ is highly dependent in other parameters such the constitutive constant C_{N10}, the external radius B and the density ρ of the solid, so the limit case for which the oscillation of the aneurysm is

attenuated by κ may be achieved when varying those parameters.

Finally, it is observed that when an internal pulsatile pressure is inserted under the conditions presented above, the aneurysm's wall reaches a limit cycle along which it will oscillate. Due to the non-linear behaviour of the aneurysm the path followed by the aneurysm will not be linear. In addition, the fact that the internal pressure is pulsatile does not affect the bifurcation of the problem but the way it oscillates. Notice that all this framework presents a non-linear model but that for sufficiently small amplitudes, it behaves as a linear one.

In conclusion, the mathematical model presented in this work is good enough to obtain an overview of which parameters affect the possible rupture of aneurysms. Whereas pressure and thickness seems to highly influence their behaviour, some others as the density of the solid and the density and viscosity of the external surrounding cerebrospinal fluid have a lower influence in the development, growth and rupture of intracranial saccular aneurysm. Moreover, the effect of a pulsatile blood flow causes the aneurysm to oscillate periodically.

6.2 Future Work

This work has presented how different biological parameters affect the behaviour of an intracranial saccular aneurysm. However, since this is a first approach in the understanding of it behaviour, it shows some limitations.

A further study of how the different parameters are affecting the model must be performed. Here the bases were set but now it has to be study how the interactions are when more than one parameter are altered. In addition, they have to be studied for a variable internal pulsatile pressure and see if bifurcations occur or not. As presented in section 5.2, κ depends in other parameters different from the viscosity. So for example, with the variation of the constitutive model's constants and the size of the aneurysm it may be the case in which the theoretical value of κ needed for strongly influence the behaviour of the problem may be achieved.

During the whole work, it has been stayed that the constitutive model is the component with more relevant influence in the dynamic behaviour of the aneurysm and that it has been developed a mathematical model valid for all spherical shell structures. Consequently, a further study using different constitutive models and comparing then with patients data is a natural step in the approach to determine the best mathematical model simulating the behaviour of an intracranial aneurysm. Moreover, much more experiments are needed in order to properly define the wall characteristics of each patient. Remember that one of the main issues of biological tissues is that many

parameters as stiffness, rigidity of the wall, thickness or even mass change continuously between biological structures but also between patients and along time. So predicting the behaviour of such structure is almost impossible without a proper characterization of the tissue itself.

Finally, some authors proposed that the rupture of an aneurysm may be caused by the resonance phenomena. This theory states that the natural frequency of the heart coincides with the natural frequency of the aneurysm and when this overlap occurs, the aneurysm breaks. Although other authors have refused this hypothesis, the nonlinearity of the problem could bring closer than expected the resonance frequencies of the aneurysm to the usual frequencies of the heart. "Nonlinear resonances of an idealized saccular aneurysm" is a further study resulted from this work that has been already submitted to the International Journal of Engineering Science and it is waiting for acceptance.

Appendix A

Derivation of Equations

A.1 Proof: Balance of Linear Momentum for a Spherical Volume Element

According to the following geometry

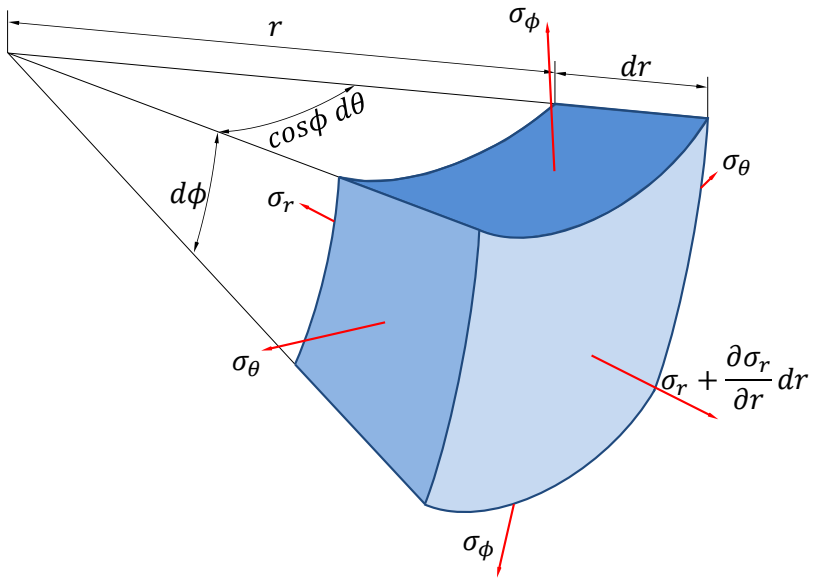

Figure A.1: Infinitesimal spherical element.

the equilibrium results as:

$$\begin{aligned}\rho r^2 \cos\phi \ddot{r} d\theta d\phi dr = \left(\sigma_r + \frac{\partial \sigma_r}{\partial r} dr\right)(r+dr)^2 \cos\phi d\theta d\phi - \sigma_r r^2 \cos\phi d\theta d\phi - \\ - 2\sigma_\phi \sin\left(\frac{d\phi}{2}\right) r \cos\phi d\theta dr - 2\sigma_\theta \sin\left(\frac{\cos\phi d\theta}{2}\right) r d\phi dr\end{aligned} \tag{A.1}$$

Due to the symmetry of the problem $\sigma_\theta = \sigma_\phi$ and for sufficiently small angles $\cos x = 1$ and $\sin x = x$. In addition, high order terms are almost zero so they are negligible:

$$\left(\sigma_r + \frac{\partial \sigma_r}{\partial r} dr\right)\left(r^2 + r dr\right) - \sigma_r r^2 - \sigma_\theta dr r - \sigma_\theta dr r = \rho r^2 \ddot{r} dr$$

Simplifying equation (A.1), the balance of linear momentum for a spherical volume element is shown in equation (A.2):

$$\boxed{\frac{\partial \sigma_r}{\partial r} + 2\frac{\sigma_r - \sigma_\theta}{r} = \rho \ddot{r}} \tag{A.2}$$

A.2 Proof: Kinematics Relationships

Applying the incompressibility condition

$$\lambda_r \lambda_\theta \lambda_\phi = 1$$

and considering that

$$\lambda_r = \frac{\partial \overline{r}}{\partial \overline{R}} \qquad , \qquad \lambda_\theta = \lambda_\phi = \frac{\overline{r}}{\overline{R}} = \lambda$$

it results that

$$J = \frac{d\overline{r}}{d\overline{R}} \left(\frac{\overline{r}}{\overline{R}} \right)^2 = 1$$

integrating along the thickness of the sphere with respect to the outer radius given that

$$A < r < B$$

where A is the inner radius and B is the outer radius, the following expression is obtained:

$$\int_r^b \overline{r}^2 d\overline{r} = \int_R^B \overline{R}^2 d\overline{R} \rightarrow r^3 - R^3 = r_b^3 - B^3$$

Considering that $\lambda = \frac{r}{R}$ and that $\lambda_b = \frac{r_b}{B}$ then

$$R^3 \left(\left(\frac{r}{R} \right)^3 - 1 \right) = B^3 \left(\left(\frac{r_b}{R_b} \right)^3 - 1 \right) \rightarrow {\lambda_b}^3 - 1 = \overline{R}^3 \left(\lambda^3 - 1 \right)$$

$$\boxed{\lambda = \sqrt[3]{1 + \frac{{\lambda_b}^3 - 1}{\overline{R}^3}}} \tag{A.3}$$

Performing the derivative with respect to $\overline{R}$ of λ:

$$\frac{d\lambda}{d\overline{R}} = \frac{1}{3} \left(1 + \frac{\lambda_b^3 - 1}{\overline{R}^3} \right)^{\frac{-2}{3}} \left(\frac{-3\overline{R}^2 \left(\lambda_b^3 - 1 \right)}{\overline{R}^6} \right) = -\frac{\lambda_b^3 - 1}{\lambda^2 \overline{R}^4}$$

and introducing ${\lambda_b}^3 - 1 = \overline{R}^3 (\lambda^3 - 1)$, the final derivative is:

$$\frac{d\lambda}{d\overline{R}} = -\frac{\lambda^3 - 1}{\lambda^2 \overline{R}}$$

Now, applying the incompressibility condition where $\frac{d\overline{r}}{d\lambda}\frac{d\lambda}{d\overline{R}}\left(\frac{\overline{r}}{\overline{R}}\right)^2 = 1$

$$\frac{d\overline{r}}{d\lambda} = \frac{\overline{R}^2}{\overline{r}^2}\frac{1}{\frac{d\lambda}{d\overline{R}}} = -\frac{\overline{R}^2}{\overline{r}^2}\frac{\lambda^2\overline{R}}{(\lambda^3 - 1)} = -\frac{\overline{R}}{\lambda^3 - 1}$$

ending with:

$$\boxed{\frac{d\lambda}{d\overline{r}} = -\frac{\lambda^3 - 1}{\overline{R}}} \tag{A.4}$$

By performing the first and second derivative of λ with respect to time

$$\dot{\lambda} = \frac{1}{3}\left(1 + \frac{\lambda_b^3 - 1}{\overline{R}^3}\right)^{\frac{-2}{3}} \frac{3\lambda_b^2 \dot{\lambda_b}}{\overline{R}^3} = \frac{\lambda_b^2 \dot{\lambda_b}}{\lambda^2 \overline{R}^3} \tag{A.5}$$

$$\begin{aligned}
\ddot{\lambda} &= -2\lambda^{-3}\dot{\lambda}\frac{\lambda_b^2\dot{\lambda}}{\overline{R}^3} + \frac{2\lambda_b \dot{\lambda_b}^2}{\lambda^2\overline{R}^3} + \frac{\lambda_b^2\ddot{\lambda_b}}{\lambda^2\overline{R}^3} = \\
&= \frac{1}{\overline{R}^3}\left(\frac{2\lambda_b\dot{\lambda_b}^2 + \lambda_b^2\ddot{\lambda_b}}{\lambda^2} - \frac{2\lambda_b^4\dot{\lambda_b}^2}{\lambda^5}\frac{\lambda^3 - 1}{\lambda_b^3 - 1}\right) = \\
&= \frac{\lambda^3 - 1}{\lambda_b^3 - 1}\left(\frac{2\lambda_b\dot{\lambda_b}^2 + \lambda_b^2\ddot{\lambda_b}}{\lambda^2} - \frac{2\lambda_b^4\dot{\lambda_b}^2}{\lambda_b^3 - 1}\frac{\lambda^3 - 1}{\lambda^5}\right)
\end{aligned} \tag{A.6}$$

and since $\lambda = \frac{\overline{r}}{\overline{R}}$ and therefore $\ddot{r} = \overline{R}\ddot{\lambda}$, joining equations (A.2) and (A.6)

$$\begin{aligned}
\frac{\partial\overline{\sigma_r}}{\partial\overline{r}} + 2\frac{\overline{\sigma_r} - \overline{\sigma_\theta}}{\overline{r}} &= \frac{\partial\overline{\sigma_r}}{\partial\lambda}\frac{\partial\lambda}{\partial\overline{r}} + 2\frac{\overline{\sigma_r} - \overline{\sigma_\theta}}{\overline{R}\lambda} = -\frac{\partial\overline{\sigma_r}}{\lambda}\frac{\lambda^3 - 1}{\overline{R}} + 2\frac{\overline{\sigma_r} - \overline{\sigma_\theta}}{\lambda\overline{R}} = \\
&= \overline{R}\frac{\lambda^3 - 1}{\lambda_b^3 - 1}\left(\frac{2\lambda_b\dot{\lambda_b}^2 + \lambda_b^2\ddot{\lambda_b}}{\lambda^2} - \frac{2\lambda_b^4\dot{\lambda_b}^2}{\lambda_b^3 - 1}\frac{\lambda^3 - 1}{\lambda^5}\right)
\end{aligned}$$

$$\frac{\partial\overline{\sigma_r}}{\partial\lambda}-2\frac{\overline{\sigma_r}-\overline{\sigma_\theta}}{\lambda\left(\lambda^3-1\right)}=\frac{\overline{R}^2}{\lambda_b^3-1}\left(\frac{2\lambda_b^4\dot{\lambda_b}^2}{\lambda_b^3-1}\frac{\lambda^3-1}{\lambda^5}-\frac{2\lambda_b\dot{\lambda_b}^2+\lambda_b^2\ddot{\lambda_b}}{\lambda^2}\right)$$

the following expression is obtained:

$$\boxed{\begin{aligned}\frac{\partial\overline{\sigma_r}}{\partial\lambda}-2\frac{\overline{\sigma_r}-\overline{\sigma_\theta}}{\lambda\left(\lambda^3-1\right)}=&\frac{\left(\lambda_b^3-1\right)^{\frac{-2}{3}}}{\left(\lambda_b^3-1\right)\left(\lambda^3-1\right)^{\frac{2}{3}}}\left(\frac{2\lambda_b^4\dot{\lambda_b}^2}{\lambda_b^3-1}\frac{\lambda^3-1}{\lambda^5}-\frac{2\lambda_b\dot{\lambda_b}^2+\lambda_b^2\ddot{\lambda_b}}{\lambda^2}\right)=\\&=\frac{2\lambda_b^4\dot{\lambda_b}^2}{\left(\lambda_b^3-1\right)^{\frac{4}{3}}}\frac{\left(\lambda-1\right)^{\frac{1}{3}}}{\lambda^5}-\frac{2\lambda_b\dot{\lambda_b}^2+\lambda_b^2\ddot{\lambda_b}}{\left(\lambda_b^3-1\right)^{\frac{1}{3}}}\frac{1}{\left(\lambda^3-1\right)^{\frac{2}{3}}\lambda^2}\end{aligned}} \tag{A.7}$$

Given that $\overline{\sigma_r}-\overline{\sigma_\theta}=-\frac{1}{2}\lambda\frac{d\overline{W}}{d\lambda}\left(\lambda^-2,\lambda,\lambda\right)$ where W corresponds with the constitutive model of the material, and that $\overline{\sigma_r}\left(\overline{r},\tau\right)=\begin{cases}\mathrm{P_a,r=inner}\\\mathrm{P_b,r=outer}\end{cases}$, if equation (A.7) is integrated along λ between the inner and the outer surface of the sphere

$$\begin{aligned}P_b-P_a+\int_{\lambda_a}^{\lambda_b}\frac{\overline{W}'}{\lambda^3-1}d\lambda=&\\=\frac{2\lambda_b^4\dot{\lambda_b^2}}{\left(\lambda_b^3-1\right)^{\frac{4}{3}}}\int_{\lambda_a}^{\lambda_b}\lambda^{-5}\left(\lambda^3-1\right)^{\frac{1}{3}}d\lambda-\frac{2\lambda_b\dot{\lambda_b}^2+\lambda_b^2\ddot{\lambda_b}}{\left(\lambda_b^3-1\right)^{\frac{1}{3}}}\int_{\lambda_a}^{\lambda_b}\frac{1}{\lambda^2\left(\lambda^3-1\right)^{\frac{2}{3}}}d\lambda=&\\=\frac{2\lambda_b^4\dot{\lambda_b^2}}{\left(\lambda_b^3-1\right)^{\frac{4}{3}}}\frac{\left(\lambda_b^3-1\right)^{\frac{4}{3}}}{4\lambda_b^4}\left(1-\frac{\lambda_b^4}{\left(\lambda_b^3+\overline{R}^3-1\right)^{\frac{4}{3}}}\right)-&\\-\frac{2\lambda_b\dot{\lambda_b}^2}{\left(\lambda_b^3-1\right)^{\frac{1}{3}}}\frac{\left(\lambda_b^3-1\right)^{\frac{1}{3}}}{\lambda_b}\left(1-\frac{\lambda_b}{\left(\lambda_b^3+\overline{R}^3-1\right)^{\frac{1}{3}}}\right)-&\\-\frac{\lambda_b^2\ddot{\lambda_b}}{\left(\lambda_b^3-1\right)^{\frac{1}{3}}}\frac{\left(\lambda_b^3-1\right)^{\frac{1}{3}}}{\lambda_b}\left(1-\frac{\lambda_b}{\left(\lambda_b^3+\overline{R}^3-1\right)^{\frac{1}{3}}}\right)&\end{aligned}$$

and considering that $f_o = \overline{R}^3$, the final governing equation is obtained:

$$\boxed{\begin{aligned} P_a(t) - P_b(t) + \int_{\lambda_a}^{\lambda_b} \frac{\overline{W}'}{\lambda^3 - 1} d\lambda = \\ = \lambda_b \ddot{\lambda_b} \left(\frac{\lambda_b}{(\lambda^3 + f_o - 1)} - 1 \right) - \dot{\lambda_b}^2 \left(\frac{\lambda_b^4}{2\left(\lambda_b^3 + f_o - 1\right)^{\frac{4}{3}}} - \frac{2\lambda_b}{\left(\lambda_b^3 + f_o - 1\right)^{\frac{1}{3}}} + \frac{3}{2} \right) \end{aligned}} \tag{A.8}$$

A.3 Proof: Pressure Exerted by the Cerebrospinal Fluid

Assuming the CSF surrounding the aneurysm to be incompressible and Newtonian [1], Navier-Stoke equations govern its behaviour. Assuming flow in the radial direction, from the continuity equation in the absence of body forces it is known that:

$$\nabla \cdot v = 0 \quad \rightarrow \quad \frac{1}{r^2}\frac{\partial}{\partial r}\left(r^2 v_r\right) = 0 \tag{A.9}$$

By integrating equation (A.9) and solving it for v_r, it results that:

$$v_r = \frac{g(t)}{r^2} \tag{A.10}$$

Since the velocity of the fluid at the aneurysm's wall matches with the velocity of the aneurysm's wall membrane

$$\frac{\partial}{\partial t}\left(u_r\right) = \frac{\partial}{\partial t}\left(b(t) - B\right) = \frac{\partial}{\partial t}\left(b(t)\right) \quad \rightarrow \quad v_r = B\dot{\lambda} \tag{A.11}$$

and knowing that $\lambda = \frac{b(t)}{B}$, joining equations (A.10) and (A.11)

$$B\dot{\lambda} = \frac{g(t)}{r^2} \quad \rightarrow \quad g(t) = \lambda\dot{\lambda}^2 B^3$$

Consequently, the final expression for the radial velocity results as:

$$v_r = \frac{B^3}{r^2}\lambda\dot{\lambda} \tag{A.12}$$

where B corresponds to the external radius of the aneurysms without deformation.

So now, consider the only non-trivial Navier-Stoke equation for the linear momentum:

$$\rho_f\left(\frac{\partial v_r}{\partial t} + v_r\frac{\partial v_r}{\partial r}\right) = -\frac{\partial p}{\partial r} + \mu\left(\frac{1}{r^2}\frac{\partial}{\partial r}\left(r^2\frac{\partial v_r}{\partial r}\right)\right) - 2\frac{\partial v_r}{\partial r}$$

[1] Newtonian fluids are those fluids for which there is a linear proportionality between the viscous stresses and the strain rates.

where ρ_f, μ and p correspond to the density, the viscosity and the pressure of the fluid respectively. If the expression for the radial velocity (equation (A.12)) is inserted:

$$\rho_f \left(\frac{\partial}{\partial t} \left(\frac{B^3}{r^2} \lambda \dot{\lambda} \right) + \left(\frac{B^3}{r^2} \lambda \dot{\lambda} \right) \frac{\partial}{\partial r} \left(\frac{B^3}{r^2} \lambda \dot{\lambda} \right) \right) = \\ = -\frac{\partial p}{\partial r} + \mu \left(\frac{1}{r^2} \frac{\partial}{\partial r} \left(r^2 \frac{\partial}{\partial r} \left(\frac{B^3}{r^2} \lambda \dot{\lambda} \right) \right) \right) - 2 \frac{\partial}{\partial r} \left(\frac{B^3}{r^2} \lambda \dot{\lambda} \right)$$

it results that:

$$\rho_f \left(\frac{B^3}{r^2} \left(\lambda^2 \ddot{\lambda}^2 + 2\lambda \dot{\lambda}^2 \right) - \frac{2B^6 \lambda^4}{r^5} \dot{\lambda}^2 \right) = -\frac{\partial p}{\partial r} \tag{A.13}$$

From before it is already known that $b = B\lambda$ being b and B the outer radius of the aneurysm deformed and non-deformed respectively. So, if expression (A.13) is integrated with respect to r between b and ∞ it results that:

$$\boxed{P_{b_f}(t) = p_\infty + \rho_f B^2 \left(\frac{3}{2} \dot{\lambda}_b^2 + \lambda_b \ddot{\lambda}_b \right)} \tag{A.14}$$

For an incompressible Newtonian fluid it is known that:

$$\sigma_{rr_s} = -p_{b_s} + 2\mu \frac{\partial v_r(t)}{\partial r}$$

Since

$$v_r(t) = \frac{B^3 \lambda_b^2 \dot{\lambda_b}}{r_b^2}$$

the final expression for the radial stress in the aneurysm's wall is:

$$\sigma_{rr_s} = -p_{b_s} + 2\mu B^3 \lambda b^2 \dot{\lambda_b} \frac{\partial}{\partial r} \left(r^{-2} \right) = -p_{b_s} + 2\mu B^3 \lambda b^2 \dot{\lambda_b} (-2) r_b^{-3}$$

Since $r_b = B\lambda_b$ and $\sigma_{rr_s} = 0$, the pressure contribution by the wall of the aneurysm is

$$\boxed{P_{b_s} = -4\mu\frac{\dot{\lambda}}{\lambda}} \tag{A.15}$$

Thus, the final pressure given by the cerebrospinal fluid is:

$$\boxed{P_b(t) = P_{b_s}(t) - P_{b_f}(t) = -p_\infty - \rho_f B^2\left(\frac{3}{2}\dot{\lambda}_b^2 + \lambda_b\ddot{\lambda}_b\right) - 4\mu\frac{\dot{\lambda}}{\lambda}} \tag{A.16}$$

A.4 Proof: Energy Terms

To obtain the energies governing the problem, multiply the non-dimensional governing equation by $2\lambda_b^2$:

$$\begin{aligned} 2\lambda_b^2\,\overline{\Delta P} = 2\lambda_b^2 \int_{\lambda_b}^{\left(\frac{\lambda_b^3+f_0-1}{f_0}\right)^{1/3}} \frac{\overline{\psi}'(\lambda)}{\lambda^3-1}\,d\lambda + 2\lambda_b^2\,4\kappa\frac{\dot{\lambda}_b}{\lambda_b} + \\ + 2\lambda_b^2\,\overline{\rho}\left(\lambda_b\ddot{\lambda}_b + \frac{3}{2}\dot{\lambda}_b^2\right) - 2\lambda_b^3\ddot{\lambda}_b\left(1-\frac{\lambda_b}{(\lambda_b^3+f_0-1)^{1/3}}\right) - \\ - 2\lambda_b^2\,\dot{\lambda_b}^2\left(\frac{3}{2}+\frac{\lambda_b^4}{2(\lambda_b^3+f_0-1)^{4/3}}-\frac{2\lambda_b}{(\lambda_b^3+f_0-1)^{1/3}}\right) \end{aligned} \tag{A.17}$$

To solve expression (A.17), it is needed to divide it in different parts. So, starting with

$$2\lambda_b^2\,\overline{\rho}\left(\lambda_b\ddot{\lambda}_b + \frac{3}{2}\dot{\lambda}_b^2\right) = \overline{\rho}\left(2\lambda_b^3\ddot{\lambda}_b + 3\lambda_b^2\dot{\lambda_b}^2\right)$$

and applying the relation presented in equation (A.18),

$$2f(x)\ddot{x} + \frac{\mathrm{d}f(x)}{\mathrm{d}x}\dot{x}^2 = \frac{\mathrm{d}}{\mathrm{d}x}\left(f(x)\dot{x}^2\right) \tag{A.18}$$

if it is considered that $f(\lambda_b) = \lambda_b^3$ and therefore, $\frac{\mathrm{d}f(\lambda_b)}{\mathrm{d}\lambda_b} = 3\lambda_b^2$, it results that:

$$\overline{\rho}\left(\dot{\lambda_b}^2\frac{\mathrm{d}f(\lambda_b)}{\mathrm{d}\lambda_b} + 2\ddot{\lambda}_b f(\lambda_b)\right) = \overline{\rho}\,\frac{\mathrm{d}}{\mathrm{d}\lambda_b}\left(f(\lambda_b)\dot{\lambda_b}^2\right);$$

$$2\lambda_b^2\,\overline{\rho}\left(\lambda_b\ddot{\lambda}_b + \frac{3}{2}\dot{\lambda}_b^2\right) = \overline{\rho}\,\frac{\mathrm{d}}{\mathrm{d}\lambda_b}\left(\lambda_b^3\dot{\lambda_b}^2\right) \tag{A.19}$$

Notice that the proof of equation (A.18) is:

$$\frac{\mathrm{d}}{\mathrm{d}x}\left(f(x)\,\dot{x}^2\right) = \dot{x}^2\frac{\mathrm{d}f(x)}{\mathrm{d}x} + f(x)\,\frac{\mathrm{d}}{\mathrm{d}x}\left(\dot{x}^2\right) = \dot{x}^2\frac{\mathrm{d}f(x)}{\mathrm{d}x} + f(x)2\ddot{x}$$

So now, taking a second part of equation (A.17),

$$\begin{aligned} 2\lambda_b^3\ddot{\lambda}_b\left(1-\frac{\lambda_b}{(\lambda_b^3+f_0-1)^{1/3}}\right)+ \\ \dot{\lambda_b}^2\left(3\lambda_b^2+\frac{\lambda_b^6}{2(\lambda_b^3+f_0-1)^{4/3}}-\frac{4\lambda_b^3}{(\lambda_b^3+f_0-1)^{1/3}}\right) \end{aligned} \tag{A.20}$$

but now considering that

$$f(\lambda_b)=\left(\lambda_b^3-\frac{\lambda_b}{\left(\lambda_b^3+f_0-1\right)^{1/3}}\lambda_b^3\right)=\lambda^3\left(1-\frac{\lambda_b}{\left(\lambda_b^3+f_0-1\right)^{1/3}}\right)$$

and that

$$\begin{aligned} \frac{\mathrm{d}}{\mathrm{d}\lambda_b}(f(\lambda_b))=\frac{\mathrm{d}}{\mathrm{d}\lambda_b}\left(\lambda_b^3-\frac{\lambda_b^4}{\left(\lambda_b^3+f_0-1\right)^{1/3}}\right)= \\ =3\lambda_b^2-\frac{4\lambda_b^3}{\left(\lambda_b^3+f_0-1\right)^{4/3}}+\frac{\lambda^6}{\left(\lambda_b^3+f_0-1\right)^{1/3}} \end{aligned}$$

equation (A.20) results as:

$$\begin{aligned} 2\lambda_b^3\ddot{\lambda}_b\left(1-\frac{\lambda_b}{(\lambda_b^3+f_0-1)^{1/3}}\right)+\frac{\mathrm{d}}{\mathrm{d}\lambda_b}\left(\lambda_b^3-\frac{\lambda_b^4}{\left(\lambda_b^3+f_0-1\right)^{1/3}}\right)= \\ =2\,f(\lambda_b)\,\ddot{\lambda_b}+\frac{\mathrm{d}}{\mathrm{d}\lambda_b}\left(f(\lambda_b)\right)\dot{\lambda_b^2}\;=\;\frac{\mathrm{d}}{\mathrm{d}x}\left(f(x)\dot{x}^2\right)\;= \\ =\frac{\mathrm{d}}{\mathrm{d}\lambda_b}\left(\left(1-\frac{\lambda_b}{(\lambda_b^3+f_0-1)^{1/3}}\right)\lambda_b^3\dot{\lambda_b^2}\right) \end{aligned} \tag{A.21}$$

Joining terms solved in equations (A.19) and (A.21) to the rest ones of equation (A.17), it results that:

$$\boxed{\begin{aligned} 2\lambda_b^2\,\overline{\Delta P}=\overline{\rho}\,\frac{\mathrm{d}}{\mathrm{d}\lambda_b}\left(\lambda_b^3\dot{\lambda_b}^2\right)+8\,\kappa\,\lambda_b\dot{\lambda_b}+ \\ +2\lambda_b^2\int_{\lambda_b}^{\left(\frac{\lambda_b^3+f_0-1}{f_0}\right)^{1/3}}\frac{\overline{\psi}'(\lambda)}{\lambda^3-1}\,\mathrm{d}\lambda-\frac{\mathrm{d}}{\mathrm{d}\lambda_b}\left(\left(1-\frac{\lambda_b}{(\lambda_b^3+f_0-1)^{1/3}}\right)\lambda_b^3\dot{\lambda_b}^2\right) \end{aligned}} \tag{A.22}$$

Finally, integrate equation (A.22) over λ between $\lambda_b(0)$ and $\lambda_{b_{max}}$, considering as initial conditions $\lambda_b(0) = 1$ and $\dot{\lambda}_b(0) = 0$ (the aneurysm is initially at rest and unstretched). Then, by performing a change of variable where $\lambda_b = \zeta$, whose integration limits transform into 1 and λ_b, the final expression for the energy terms is:

$$\boxed{\begin{aligned} 2\overline{\Delta P}\frac{\lambda_b^3-1}{3} &= \overline{\rho}\lambda_b^3\dot{\lambda}_b^2 + 8\kappa\int_1^{\lambda_b}\lambda_b\dot{\lambda}_b\mathrm{d}\zeta + \\ &+ 2\int_1^{\lambda_b}\lambda_b^2\int_{\lambda_b}^{\left(\frac{\lambda_b^3+f_0-1}{f_0}\right)^{1/3}}\frac{\overline{\psi}'(\lambda)}{\lambda_b^3-1}\,\mathrm{d}\lambda\,\mathrm{d}\zeta - \lambda_b^3\dot{\lambda}_b^{\,2}\left(1-\frac{\lambda_b}{(\lambda_b^3+f_0-1)^{1/3}}\right) \end{aligned}} \tag{A.23}$$

From this expression it can be deduced the final balance of mechanical energy is:

$$\overline{\Pi_e} = \overline{\Pi_s} + \overline{\mathcal{K}_s} + \overline{\mathcal{K}_f} + \overline{\mathcal{D}_f}$$

where

$$\overline{\Pi_e} = 2\overline{\Delta P}\frac{\lambda_b^3-1}{3} \tag{A.24a}$$

$$\overline{\Pi_s} = 2\int_1^{\lambda_b}\lambda_b^2\int_{\lambda_b}^{\left(\frac{\lambda_b^3+f_0-1}{f_0}\right)^{1/3}}\frac{\overline{\psi}'(\lambda)}{\lambda_b^3-1}\,\mathrm{d}\lambda\,\mathrm{d}\zeta \tag{A.24b}$$

$$\overline{\mathcal{K}_s} = -\lambda_b^3\dot{\lambda}_b^{\,2}\left(1-\frac{\lambda_b}{(\lambda_b^3+f_0-1)^{1/3}}\right) \tag{A.24c}$$

$$\overline{\mathcal{K}_f} = \overline{\rho}\lambda_b^3\dot{\lambda}_b^2 \tag{A.24d}$$

$$\overline{\mathcal{D}_f} = 8\kappa\int_1^{\lambda_b}\lambda_b\dot{\lambda}_b\mathrm{d}\zeta \tag{A.24e}$$

where $\overline{\Pi_e}$ is the work done by the external forces, $\overline{\Pi_s}$ the elastic energy stored by the aneurysm's wall, $\overline{\mathcal{K}_s}$ the kinetic energy of the aneurysm, $\overline{\mathcal{K}_f}$ the kinetic energy of the CSF and $\overline{\mathcal{D}_f}$ the viscous dissipation given by the surrounding CSF.

Since the viscous dissipation cannot be integrated along the stretch, a change of variable is performed in order to integrate it along time. For that, considering that $\mathrm{d}\lambda_b = \dot{\lambda_b}\mathrm{d}\xi$, the final expressions for the energies governing the problem are:

$$\overline{\Pi_e} = 2\overline{\Delta P}\frac{\lambda_b^3 - 1}{3} \tag{A.25a}$$

$$\overline{\Pi_s} = 2\int_0^\tau \lambda_b^2\dot{\lambda}_b \int_{\lambda_b}^{\left(\frac{\lambda_b^3+f_0-1}{f_0}\right)^{1/3}} \frac{\overline{\psi}'(\lambda)}{\lambda_b^3 - 1}\,\mathrm{d}\lambda\,\mathrm{d}\xi \tag{A.25b}$$

$$\overline{\mathcal{K}_s} = -\lambda_b^3\dot{\lambda_b}^2\left(1 - \frac{\lambda_b}{(\lambda_b^3 + f_0 - 1)^{1/3}}\right) \tag{A.25c}$$

$$\overline{\mathcal{K}_f} = \overline{\rho}\lambda_b^3\dot{\lambda}_b^2 \tag{A.25d}$$

$$\overline{\mathcal{D}_f} = 8\kappa\int_0^\tau \lambda_b\dot{\lambda}_b^2\mathrm{d}\xi \tag{A.25e}$$

Appendix B

Regulatory Framework and Budget

B.1 Regulatory Framework

Bio-research has brought into discussion some issues that were unthinkable even a few decades ago. The question of whether experimentation with human beings is ethical or not has been extensively discussed during the last century, though an agreement has not been achieved yet. Depending on their beliefs, traditions and culture, each country has a different legislation, and even within countries people hold debates about these issues. For some people, experimenting with some parts of the body is a crime and should be strictly forbidden, whereas for others it is just a natural step in human evolution and should be promoted, and a great diversity of opinions can be found in between. What it remains a truth is that science needs from human research in order to advance in a great variety of fields such as regenerative medicine or prosthetics. In fact, human research would be a required step in order to validate the mathematical model presented in this work.

In general, there is a consensus that research with human subjects must ensure the integrity of individuals under study and should never compromise their lives and aptitudes. Even if some research works could save thousands of lives if they crossed some of these boundaries, for many people this research would remain unethical, and the community is not willing to accept it. Probably it is a matter of time that some alternatives to humans for clinical trials will appear but until that moment, some regulations are needed in order to ensure humans rights.

Although this project is not directly affected by any specific regulation, it has established a need for clinical experimentation in order to validate the mathematical model.

The need of contrasting the data obtained with real subjects suffering from intracranial saccular aneurysms and of performing further experimentation to get the appropriate constitutive models that will fit this model entails many considerations. Consequently, different regulations can be found affecting mainly two groups of subjects: dead subjects and living subjects.

Dead subjects

In Spain, the use of parts or the whole body of a death individual is regulated at a country-level, although each region has further legislation. There is no specific regulations for donations of corpses for teaching or anatomic research [19]. However, with respect to the use of human tissue, the law "Real Decreto 411/1996, de 1 de marzo, por el que se regulan las actividades relativas a la utilización de tejidos humanos" [37] establishes the use of human tissues for therapy, teaching and research always respecting the fundamental rights of an individual and the ethics concerning the biomedical research. By this way, the use of intracranial saccular aneurysms coming from autopsies could be employed for performing some constitutive tests and fit the parameters to already existing models or even developing some new models that describe the behaviour of these aneurysms.

Living subjects

Legislation is more strict when it involves living subjects. According to "Ley 41/2002, de 14 de noviembre, básica reguladora de la autonomía del paciente y de derechos y obligaciones en materia de información y documentación clínica" [29], every patient has the right to use the methods employed in a research project and in any case it will not conform an extra risk for his health. Furthermore, all subjects involved in clinical research must be appropriately informed and they will freely and voluntary decide about their participation, requiring an explicit consent. Nevertheless in the experiments proposed in this project, no further legislation will be needed since it is just a matter of comparing information and it does not involve any procedure that may endanger humans integrity.

B.2 Budget

Due to the remarkable theoretical character of this work, the weight of the budget does not resides in any material expenses but in the personal required the project. So the expected expenses are going to be presented below.

In table B.1, two sections are presented. The first one includes all the expenses in human resources i.e., the salaries per hour for each member of the research project, which includes a project manager, a research assistant and a bachelor student. The second consist in the materials expenses. Notice that the prize for the computer is calculated with a lineal depreciation. So, in case the computer costs €1200 and that it has an expected life time of 4 years, the price per year will be of €600. Then, the price selected for the Matlab license [35] is that one corresponding with the academic use for a single individual. Finally, the concept of consumables includes the papers and pens employed for thinking and deriving the equations and the ink expenses, needed for printing bibliography and the final bachelor thesis itself.

Human resources

Concept	**Unit price (€/h)**	**Hours**	**Total cost (€)**
Project manager	120	80	9600
Research assistant	60	80	4800
Student	20	400	8000
		Subtotal	22400

Materials

Concept	**Unit price (€)**	**Qty.**	**Total cost (€)**
Computer	300 / year	2	600
MATLAB license	500 / year	2	1000
Consumables	100 / year	2	200
		Subtotal	1800
		Total	24200

Figure B.1: Detailed budget for the current project.

References

[1] Akkas, N. *Biomechanical Transport Processes*. Springer, 1990. Chapter: Aneurysms as a biomechanical instability problem.

[2] Anderson, C. S., Feigin, V., Bennett, D., Lin, R.-B., Hankey, G., and Jamrozik, K. Active and passive smoking and the risk of subarachnoid hemorrhage: An international population-based case-control study. *Stroke 35*, 3 (2004), 633–637.

[3] Asaithambi, G., Adil, M. M., Chaudhry, S. A., and Qureshi, A. I. Incidences of unruptured intracranial aneurysms and subarachnoid hemorrhage: results of a statewide study. *Journal of Vascular and Interventional Neurology 14* (2014), 14–17.

[4] Asari, S., and Ohmoto, T. Natural history and risk factors of unruptured cerebral aneurysms. *Clinical Neurology and Neurosurgery 95* (1993), 205–214.

[5] Austin, G., Schievink, W., and Williams, R. Controlled pressure-volume factors in the enlargement of intracranial aneurysms. *Neurosurgery 24*, 5 (1989), 722–730.

[6] Bloomfield, I., Johnston, I., and Bilston, L. Effects of proteins, blood cells and glucose on the viscosity of cerebrospinal fluid. *Pediatric Neurosurgery 28*, 5 (1998), 246–251.

[7] Bonita, R. Cigarette smoking, hypertension and the risk of subarachnoid hemorrhage: a population-based case–control study. *Stroke 17*, 5 (1986), 831–835.

[8] Brain Aneurysm Foundation. Brain aneurysm basics, 2017. `https://www.bafound.org/about-brain-aneurysms/brain-aneurysm-basics/`; last visited on 2017-06-12.

[9] Cebral, J. R., and Raschi, M. Suggested connections between risk factors of intracranial aneurysms: A review. *Annals of Biomedical Engineering 41*, 7 (2013), 1366–1383.

[10] Challa, V., and Han, H.-C. Spatial variations in wall thickness, material stiffness and initial shape affect wall stress and shape of intracranial aneurysms. *Neurological Research 29* (2007), 569–577.

[11] Chalouhi, N., Ali, M. S., Jabbour1, P. M., Tjoumakaris, S. I., Gonzalez, L. F., Rosenwasser, R. H., Koch, W. J., and Dumont, A. S. Biology of intracranial aneurysms: role of inflammation. *Journal of Cerebral Blood Flow & Metabolism 32* (2012), 1659–1676.

[12] Chalouhi, N., Hoh, B. L., and Hasan, D. Review of cerebral aneurysm formation, growth and rupture. *Journal of the American Heart Association 40* (2013), 3613–3622.

[13] Costalat, V., Sanchez, M., Ambard, D., Thines, L., Lonjon, N., Nicoud, F., Brunel, H., Lejeune, J. P., Dufour, H., Bouillot, P., Lhaldky, J. P., Kouri, K., Segnarbieux, F., Maurage, C. A., Lobotesis, K., Villa-Uriol, M. C., Zhang, C., Frangi, A. F., G., M., Bonafé, A., Sarry, L., and Jourdan, F. Biomechanical wall properties of human intracranial aneurysms resected following surgical. *Journal of Biomechanics 44*, 15 (2011), 2685–2691.

[14] David, G., and Humphrey, J. D. Further evidence of the dynamic stability of intracranial saccular aneurysms. *Journal of Biomechanics 36* (2003), 1143–1150.

[15] Etminan, N., and Rinkel, G. J. Unruptured intracranial aneurysms: development, rupture and preventive management. *Nature Reviews Neurology 12* (2016), 699–713.

[16] Ferguson, G. G. Direct measurement of mean and pulsatile blood pressure at operation in human intracranial saccular aneurysms. *Journal of Neurosurgery 36*, 5 (1972), 560–563.

[17] Ferguson, G. G. Physical factors in the initiation, growth, and rupture of human intracranial saccular aneurysms. *Journal of Neurosurgery 37* (1972), 666–677.

[18] Frosen, J., Tulamo, R., Paetau, A., Laaksamo, E., Korja, M., Laakso, A., Niemela, M., and Hernesniemi, J. Saccular intracranial aneurysm: pathology and mechanisms. *Acta Neuropathology 123* (2012), 773–786.

[19] González-López, E., and Cuerda-Galindo, E. La utilización de cadáveres y órganos en la investigación y docencia médica. lecciones de la historia. *Medicine Clínica 138*, 10 (2012), 441–444.

[20] Green, A., and Zerna, W. *Theoretical Elasticity*. Dover, 1992. Chapter: General Theory of Membrane Shells.

[21] Hackett, R. M. *Hyperelasticity Primer*. Springer, 2016. Chapter 4: Strain-Energy Functions.

[22] Haslach, H. W., and Humphrey, J. D. Dynamics of biological soft tissue and rubber: internally pressurized spherical membranes surrounded by a fluid. *International Journal of Non-Linear Mechanics 39*, 3 (2004), 399–420.

[23] Humphrey, J. D., H. H. W. *Wall/Fluid Interactions in Physiologic Flows*. WIT Press, 2003. Chapter: Elastodynamics of saccular aneurysms: solid-fluid interactions and constitutive relations.

[24] Humphrey, J. D., and DeLange, S. *An Introduction to Biomechanics: Solids and Fluids, Analysis and Design*. Springer, 2004.

[25] Hung, E. J., and Botwin, M. R. Mechanics of rupture of cerebral saccular aneurysms. *Journal of Biomechanics 8*, 6 (1975), 385–392.

[26] Investopedia. Gross domestic product - gdp, 2017. `http://www.investopedia.com/terms/g/gdp.asp`; last visited on 2017-06-12.

[27] Isaksen, J. G., Bazilevs, Y., Kvamsdal, T., Zhang, Y., Kaspersen, J. H., Waterloo, K., Romner, B., and Ingebrigtsen, T. Determination of wall tension in cerebral artery aneurysms by numerical simulation. *Stroke 39* (2008), 3172–3178.

[28] Jain, J. Mechanism of rupture in intracranial saccular aneurysms. *Surgery 54*, 2 (1963), 347–350.

[29] Jefatura del Estado. Ley 41/2002, de 14 de noviembre, básica reguladora de la autonomía del paciente y de derechos y obligaciones en materia de información y documentación clínica. Boletín Oficial del Estado.

[30] Joseph, R. G. Stroke and cerebral vascular disease thrombi, emboli, transient ischemic attacks, hemorrhage, aneurysms, atherosclerosis... `http://brainmind.com/BrainLecture12.html`; last visited on 2017-06-19.

[31] Krings, T., Mandell, D. M., Kiehl, T.-R., Geibprasert, S., Tymianski, M., Alvarez, H., terBrugge, K. G., and Hans, F.-J. Determination of wall tension in cerebral artery aneurysms by numerical simulation. *Nature Reviews Neurology 7* (2011), 547–559.

[32] Levin, E., Muravchick, S., and Gold, M. I. Density of normal human cerebrospinal fluid and tetracaine solutions. *Anesthesia and Analgesia 60*, 11 (1981), 814–817.

[33] Lindekleiv, H. M., Valen-Sendstad, K., Morgan, M. K., Mardal, K.-A., Faulder, K., Magnus, J. H., Waterloo, K., Romner, B., and In-

GEBRIGTSEN, T. Sex differences in intracranial arterial bifurcations. *Gender Medicine 7*, 2 (2010), 149–155.

[34] MACDONALD, D. J., FINLAY, H. M., AND CANHAM, P. B. Directional wall strength in saccular brain aneurysms from a polarized light microscopy. *Annals of Biomedical Engineering 28* (2000), 533–542.

[35] MATHWORKS. Pricing and licensing, 2017. `https://es.mathworks.com/pricing-licensing.html?prodcode=ML&intendeduse=edu`; last visited on 2017-06-17.

[36] MENG, H., TUTINO, V., XIANG, J., AND SIDDIQUI, A. High wss or low wss? complex interactions of hemodynamics with intracranial aneurysm initiation, growth, and rupture: Toward a unifying hypothesis. *American Journal of Neuroradiology 35*, 7 (2014), 1254–1262.

[37] MINISTERIO DE SANIDAD Y CONSUMO. Real decreto 411/1996, de 1 de marzo, por el que se regulan las actividades relativas a la utilización de tejidos humanos. Boletín Oficial del Estado.

[38] MINYARD, A. N., AND PARKER, J. C. Intracranial saccular (berry) aneurysm: A brief overview. *Southern Medical Journal 90*, 7 (1997), 672–678.

[39] NATIONAL HEART, LUNG AND BLOOD INSTITUTE. Types of aneurysms, 2011. `https://www.nhlbi.nih.gov/health/health-topics/topics/arm/types`; last visited on 2017-05-26.

[40] OGDEN, R. *Non-linear Elastic Deformations*. Dover Civil and Mechanical Engineering. Dover Publications, 1997.

[41] OTTOSEN, N. S., AND RISTINMAA, M. *The Mechanics of Constitutive Modeling*. Oxford [etc.] : Elsevier, 2005.

[42] PARK, D.-H., KANG, S.-H., LEE, J.-B., LIM, D.-J., KWON, T.-H., CHUNG, Y.-G., AND LEE, H.-K. Angiographic features, surgical management and outcomes of proximal middle cerebral artery aneurysms. *Clinical Neurology and Neurosurgery 110*, 6 (2008), 544–551.

[43] QUEZADA-GARCÍA, M., AND HUETE-GARCÍA, A. Magnitud del Daño Cerebral Adquirido en España y en Castilla La-Mancha. *Fundación Tutelar Daño Cerebral Castilla-La Mancha* (2013), 1–52.

[44] RYAN, J., AND HUMPHREY, J. Finite element based predictions of preferred material symmetries in saccular aneurysms. *Annals of Biomedical Engineering 27*, 5 (1999), 641–647.

[45] Sadasivan, C., Fiorella, D. J., Woo, H. H., and Lieber, B. B. Physical factors effecting cerebral aneurysm pathophysiology. *Annals of Biomedical Engineering 41*, 7 (2013), 1347–1365.

[46] Sekhar, L. N., and Heros, R. C. Growth, origin and rupture of saccular aneurysms: A review. *Neurosurgery 8*, 2 (1981), 248–260.

[47] Sekhar, L. N., Sclabassi, R. J., Sun, M., Blue, H. B., and Wasserman, J. F. Growth, origin and rupture of saccular aneurysms: A review. *Stroke 19*, 3 (1988), 352–356.

[48] Shah, A. D., and Humphrey, J. D. Finite strain elastodynamic of intracranial saccular aneurysms. *Journal of Biomechanics 32* (1999), 593–599.

[49] Simkins, T., and Stehbens, W. Vibrational behavior of arterial aneurysms. *Letters in Applied and Engineering Sciences 1*, 85 (1973), 100.

[50] Singh, P. K., Marzoc, A., Howardd, B., Rufenachte, D. A., Bijlengaf, P., Frangig, A. F., Lawfordc, P. V., Coleyj, S. C., Hosec, D. R., and Pate, U. J. Effects of smoking and hypertension on wall shear stress and oscillatory shear index at the site of intracranial aneurysm formation. *Clinical Neurology and Neurosurgery 112*, 4 (2010), 306–313.

[51] Suzki, J., and Ohara, H. Clinicopathological study of cerebral aneurysms. *Journal of Neurosurgery 48* (1978), 505–514.

[52] Tortora, G. J., and Derrickson, B. *Principles of Anatomy & Physiology*, 13th ed. John Wiley & Sons, 2012.

[53] Valencia, C., Villa-Uriol, M., Pozo, J., and Frangi, A. Morphological descriptors as rupture indicators in middle cerebral artery aneurysms. *Procedings of 2010 IEEE-EMBS 41*, 7 (2010), 6046–6049.

[54] Villablanca, J. P., Duckwiler, G. R., Jahan, R., Tateshima, S., Martin, N. A., Frazee, J., Gonzalez, N. R., Sayre, J., and Vinuela, F. V. Natural history of asymptomatic unruptured cerebral aneurysms evaluated at ct angiography: Growth and rupture incidence and correlation with epidemiologic risk factors. *Radiology 269*, 1 (2013).

[55] Vlak, M. H. M., Algra, A., Brandenburg, R., and Rinkel, G. J. E. Prevalence of unruptured intracranial aneurysms, with emphasis on sex, age, comorbidity, country, and time period: a systematic review and meta-analysis. *The Lancet Neurology 10*, 7 (2011), 626–636.

[56] Watton, P. N., Selimovic, A., Raberger, N. B., Huang, P., Holzapfel, G. A., and Ventikos, Y. Modelling evolution and the evolving mechani-

cal environment of saccular cerebral aneurysms. *Biomechanics and Modeling in Mechanobiology 10* (2011), 109–132.

[57] Wiebers, D. O., Torner, J. C., and Meissner, I. Impact of unruptured intracranial aneurysms on public health in the united states. *Stroke 23*, 10 (1992), 1416–1419.

[58] Williams, B., Poulter, N., Brown, M., Davis, M., McInnes, G., Potter, J., Sever, P., and Thom, S. M. Guidelines for management of hypertension: report of the fourth working party of the british hypertension society, 2004—bhs iv. *Journal of Human Hypertension 18* (2004), 139–185.